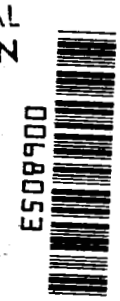

NASA
Technical
Paper
2187

September 1983

Experimental and Analytical Investigation of the Fracture Processes of Boron/Aluminum Laminates Containing Notches

W. S. Johnson,
C. A. Bigelow, and
Y. A. Bahei-El-Din

25th Anniversary
1958-1983

NASA
Technical
Paper
2187

1983

Experimental and Analytical Investigation of the Fracture Processes of Boron/Aluminum Laminates Containing Notches

W. S. Johnson
and C. A. Bigelow
Langley Research Center
Hampton, Virginia

Y. A. Bahei-El-Din
University of Cairo
Cairo, Egypt

NASA
National Aeronautics
and Space Administration

**Scientific and Technical
Information Branch**

SUMMARY

The purpose of this report is to enhance understanding of the fracture process of metal matrix composites, boron/aluminum composites specifically. These composites experience widespread yielding of the matrix material during the fracture process. This plasticity complicates the analysis of the composites containing notches. This report presents experimental results for five laminate orientations of boron/aluminum composites containing either circular holes or crack-like slits. Specimen stress-strain behavior, stress at first fiber failure, and ultimate strength were determined. Radiographs were used to monitor the fracture process. The specimens were analyzed with a three-dimensional elastic-plastic finite-element model.

The first fiber failures in notched specimens with $[\pm 45]_{2s}$, $[0/\pm 45]_{s}$, and $[0_2/\pm 45]_{s}$ laminate orientations occurred at or very near the specimen ultimate strength. For notched unidirectional specimens, the first fiber failure occurred at approximately one-half of the specimen ultimate strength. Acoustic emission events correlated with fiber breaks in unidirectional composites, but did not for other laminates. Circular holes and crack-like slits of the same characteristic length were found to produce approximately the same strength reduction. The predicted stress-strain responses and stress at first fiber failure compared very well with test data for laminates containing 0° fibers and reasonably well for $[\pm 45]_{2s}$ laminates.

INTRODUCTION

Metal matrix composites have several inherent properties, such as high stiffness-to-weight ratios and high strength-to-weight ratios, which make them attractive for structural applications. These composites also have greater transverse strength, a higher operating temperature range, and better environmental resistance than current epoxy-resin-matrix composites. Like polymer matrix composites, however, metal matrix composites are very notch sensitive. The degree of this sensitivity depends on the notch size and shape, as well as the laminate orientation. Unlike typical polymer matrix composites, metal matrix composites may exhibit widespread yielding of the matrix before laminate failure. To design damage-tolerant structures (or to simply understand the effects of fastener holes), the laminate fracture strength must be known for a wide range of ply orientations, notch geometries, and loading conditions. Furthermore, a method for predicting fracture strength is needed to avoid testing all laminate, notch, and loading combinations of interest.

The purpose of this research was to investigate the fracture process of boron/aluminum (B/Al) composites containing circular holes and crack-like slits. B/Al composites with slits had already been tested and fracture data published (ref. 1). To further understanding of the B/Al fracture process, four laminate orientations of B/Al composites with circular holes were tested during the present investigation. One unidirectional monolayer specimen with a center slit was also tested. Stress and overall strain data were obtained from initial loading to laminate failure, and the specimens were radiographed periodically during loading to record damage initiation and propagation.

A three-dimensional elastic-plastic finite-element analysis program was modified to analyze the mechanical behavior of the specimens. Overall stress-strain responses and first fiber failures were predicted for the notched specimens. To evaluate the analysis, the elastic-plastic predictions were compared with experimental data.

SYMBOLS

AE	acoustic emission
a	half-length of slit or radius of circular hole, m
S	laminate stress, MPa
v_f, v_m	volume fractions of fibers and matrix
w	specimen width, mm
x_i	Cartesian coordinates (i = 1, 2, 3)
$\bar{x}_i$	material coordinates (i = 1, 2, 3)
ε	constituent strain tensor, m/m
$\bar{\varepsilon}$	overall laminate strain tensor, m/m
σ	constituent stress tensor, MPa
$\bar{\sigma}$	overall laminate strain tensor, MPa

Subscripts:

f	fiber
m	matrix
ult	ultimate
1,2	transverse directions
3	0° fiber, or axial, direction

EXPERIMENTS

A considerable amount of experimental fracture data have been generated during the past decade. References 2 to 4 are good examples. The past tests focused primarily on the development of stress-strain response data and laminate ultimate strength. The process of fracture (i.e., when damage first initiates and how it grows under increasing static load) has not been investigated. Therefore, the purpose of the experimental tests presented in this report is to characterize the fracture process. The overall stress-strain response and laminate failure load were, of course, recorded.

Material and Specimens

The B/Al laminates were made by diffusion-bonding sheets of 0.142-mm-diameter boron fibers and 6061 aluminum foil. The laminates were used in the "as fabricated" condition; that is, they were not heat treated. The laminate orientations were $[0]_6$, $[0_2/\pm45]_s$, $[0/\pm45]_s$, and $[\pm45]_{2s}$. The fiber volume fractions were 0.50 for the $[0]_6$ laminate and 0.45 for the other laminates. Fracture and tensile specimens were cut from each sheet of material. The tensile specimens had been previously tested by Sova and Poe (ref. 5) to measure tensile stress-strain behavior for unnotched laminates. Fracture specimens containing crack-like slits had also been tested previously by Poe and Sova (ref. 1).

The fracture specimens tested in this study were 51 and 102 mm wide. Circular holes were machined at the center of each fracture specimen with an ultrasonic rotary diamond-impregnated-core drill. The diameter of the holes ranged from 3.18 to 25.4 mm. Table I lists hole diameters for each specimen width. The sketch of the fracture specimen in figure 1 identifies fiber orientation angles and the location of the linearly varying displacement transducer (LVDT) used to measure specimen elongation.

One specimen consisting of a monolayer of unidirectional B/Al was also tested. The monolayer, 76 mm wide, contained a center crack-like slit 19 mm long and had a fiber volume fraction of 0.30.

Test Procedure and Equipment

The specimens were tested in a hydraulically actuated, closed-loop, servo-controlled testing machine. The load, measured by a conventional load cell, was used for the feedback signal. In addition, some tests were strain controlled. The loads (or strains) were programmed by an analog ramp generator to vary linearly with time. The applied load and the overall strain as measured from the LVDT were recorded on an X-Y plotter. The overall strain is the displacement measured by the LVDT (fig. 1) divided by 89 mm.

During several tests, specimens were radiographed with an industrial-type "soft" X-ray machine with a 0.25-mm-thick beryllium window and a tungsten target. The voltage was set at 50 kV and the current at 20 mA. The window of the X-ray tube was 300 mm from the specimen. A Kodak high resolution photographic plate (type 1A) was mounted to the specimen on the opposite side. Exposure time was about 5 minutes. The load (or strain) was held constant during each radiograph.

Specimens were radiographed either at several increments of load or when damage growth was indicated by acoustic emission (AE) signals. Acoustic emission signals were also recorded during these tests. A Dunegan/Endevco 3000 series AE system monitored the AE events that had peak amplitudes above 65 dB. These AE events were compared with the radiographs to correlate the fiber breaks with the acoustic emissions.

Test Results and Discussions

Monolayer test.- Figure 2 shows a series of radiographs taken at increasing load levels applied to the monolayer test specimen. Only the left end of the center slit is shown. The dark, thin lines in the radiographs are the tungsten cores of the boron fibers. The light area around the tungsten core is the boron. The gray area

between is the aluminum matrix. Obviously, the fibers are not uniformly spaced. As the specimen was slowly loaded, the number of AE events in the range from 65 to above 100 dB were recorded for each radiograph taken.[1] The number of events above 100 dB was compared with the number of fibers broken.

Figure 2(a) shows the specimen at a stress level of 196 MPa with no apparent fiber failure nor any AE events above 100 dB. At a stress level of 216 MPa, a single event above 100 dB was recorded and one broken fiber was observed at the right end of the slit. Figure 2(b) shows two broken fibers at the notch tip at a stress level of 237 MPa. Two AE events above 100 dB were recorded. Figure 2(c) shows six broken fibers with three AE events above 100 dB. Acoustic emission equipment may not record the sound of every fiber break, especially if breaks occur nearly simultaneously. Figure 2(c) clearly shows that the boron fibers break before matrix failure. This is because the fibers have a 0.6 percent strain to failure, whereas the matrix material has more than 7.5 percent strain to failure. Figure 2(d) shows the damage state just before failure; there were 27 broken fibers and 11 AE events above 100 dB.

The results of the test of the monolayer specimen indicated a qualitative correlation between the AE events above 100 dB and the 0° fiber breaks for unidirectional laminates. The monolayer test illustrated that the boron fibers fail well in advance of the matrix material. Fiber failure first occurred at a stress of approximately 60 percent of the ultimate load. The crack grew in a self-similar manner until the specimen failed.

The $[0]_6$ tests.- Nine $[0]_6$ laminate specimens with circular holes were loaded to failure. The gross section ultimate stress for each specimen plotted versus the ratio of hole diameter to specimen width (2a/w) is shown in figure 3. The two specimen widths are distinguished by open and closed symbols. Also plotted in figure 3 are the ultimate strength data obtained from similar specimens containing crack-like slits (ref. 1), for which 2a/w is the ratio of slit length to specimen width. The curve for the net section ultimate strength was found by multiplying the unnotched tensile strength of the laminate by (1 - 2a/w). This curve represents the specimen gross stress that corresponds to a net section stress equal to the unnotched tensile strength of the laminate. The unnotched tensile strengths were determined by Sova and Poe (ref. 5) and are listed in table II for each layup. The strength data and the curve for net section ultimate strength differ because of the notch effect. Note that at a given value of 2a/w, the ultimate stresses are nearly the same for specimens with holes and with slits. As a result, the notch effect appears to be a function of notch length rather than the notch radius or width. This may be attributed to the widespread yielding that occurs near the notch long before the failing load is reached. Examples of the yield patterns are presented in the analytical section. The wider specimens failed at a lower laminate stress for the same value of 2a/w.

Figure 4 shows a series of four radiographs of the $[0]_6$ laminate and the associated number of AE events above 100 dB. The arrow in figure 4(a) indicates the region of developing damage, shown as light areas indicating breaks in the fibers near the edge of the hole. This damage was more evident in the original radiographs. Other apparent fiber damage around the hole was caused by machining and was present at the beginning of the test. A radiograph was taken at a slightly lower load than fig-

[1]The dB levels are a function of the basic AE unit and transducer used. A Dunegan/Endevco S 750B transducer was used with a model 1801 preamplifier which contained a 450B band-pass filter.

ure 4(a). There were no AE events and no evidence of fiber failure. The first AE event above 100 dB corresponded to the first observed fiber damage. The number of fiber breaks increased with additional AE events. Again, the AE events gave a good qualitative indication of fiber damage. The first fiber failure observed was at approximately 40 percent of the ultimate laminate stress in the location indicated by the arrow. As in the monolayer specimen, the damage propagated in a self-similar manner until failure, as can be seen in figures 4(a) through 4(d).

The $[\pm 45]_{2s}$ tests.- Eight $[\pm 45]_{2s}$ laminate specimens with circular holes were loaded to failure. The ultimate strength of each specimen is plotted versus 2a/w in figure 5. The strengths of specimens containing crack-like slits (ref. 1) are also plotted. There does not appear to be a close correlation between slit and hole data as was observed in figure 3 for the $[0]_6$ laminates. This lack of correlation may be attributed to relative scatter in the strength data, possibly due to widespread matrix yielding. The actual range of scatter (i.e., 100 MPa) is about the same as for the $[0]_6$ specimens; however, the absolute value of strength is much lower for the $[\pm 45]_{2s}$ specimens.

The unnotched tensile strength of the $[\pm 45]_{2s}$ laminates was very width dependent, as shown in table II. No width dependency was found for the unnotched tensile strength of the other layups tested (ref. 1). Two net section strength lines are shown in figure 5 for 102-mm-wide and 51-mm-wide specimens.

Radiographs were taken of several specimens during testing. Figure 6 shows the typical failing sequence during loading and the accompanying AE events. The specimen shown was tested under strain control. First fiber failure was not observed until the laminate was loaded to 95 percent of its ultimate strength, as shown in figure 6(a). Notice that 350 AE events above 100 dB had accumulated at this stress level, yet only two broken fibers could be seen. AE events above 100 dB and broken fibers do not seem to correlate for the $[\pm 45]_{2s}$ laminates. Perhaps these AE events were caused by fiber-matrix separation. Figure 6(c) shows the critical damage state at maximum stress level. If load control had been used, specimen fracture would have occurred at the damage state shown in figure 6(c). Figure 6(d) shows unstable damage growth occurring at a 45° angle.

The $[0/\pm 45]_s$ tests.- Eight $[0/\pm 45]_s$ laminate specimens with circular holes were loaded to failure. The ultimate laminate stress for each specimen is plotted versus 2a/w in figure 7. The hole data again agree very closely with the slit data of Poe and Sova (ref. 1). Like the $[0]_6$ laminates, the wider specimens failed at a lower laminate stress for the same value of 2a/w.

Radiographs of specimens were taken at increasing load levels approaching the ultimate strength. The radiographs showed no signs of fiber failure prior to laminate failure. Presumably, the fibers all failed in rapid sequence at the ultimate load. Acoustic emission events were recorded at load levels above 25 percent of the ultimate load, yet no fiber failures were observed.

The $[0_2/\pm 45]_s$ tests.- Nine $[0_2/\pm 45]_s$ laminate specimens with circular holes were loaded to failure. Figure 8 presents the ultimate laminate strength plotted versus 2a/w for each specimen. As previously noted for the $[0]_6$ and $[0/\pm 45]_s$ laminates, the $[0_2/\pm 45]_s$ laminates with holes and with slits exhibited virtually no difference in ultimate strengths, but notch length did have an effect.

Radiographs were also taken of a $[0_2/\pm 45]_s$ laminate near the ultimate stress. As for the $[0/\pm 45]_s$ laminates, no fiber failures were observed before laminate fail-

ure. Again, many AE events above 100 dB were recorded throughout the tests, but none seemed to correlate with fiber failures.

Summary of Experimental Data

In summary, the experimental phase of the investigation indicated the following:

1. First fiber failure occurred very near the ultimate notched laminate strength (within 5 percent) for $[\pm 45]_{2s}$, $[0/\pm 45]_s$, and $[0_2/\pm 45]_s$ B/Al laminates containing holes. Unidirectional laminates with holes experienced first fiber failures at approximately 50 percent of ultimate laminate stress. Poe and Sova (ref. 1) and Jones (ref. 6) found similar results for B/Al laminates containing crack-like slits.

2. Acoustic emission events correlated with fiber breaks in unidirectional laminates, but did not for other laminate orientations.

3. The ultimate strength decreased with increased specimen notch length (slit length or hole diameter).

ANALYTICAL MODELING OF FIBROUS COMPOSITES

In aluminum matrix composites the matrix yields, whereas the fibers generally behave elastically until they break. Therefore, to model the behavior of metal matrix composites, the elastic-plastic behavior of the matrix and the elastic behavior of the fiber must be accounted for. An analysis that models this two-phase behavior with any specimen configuration and incorporates fiber and matrix failure was developed in the present study. The analysis used is a three-dimensional finite-element program (ref. 7) called PAFAC (plastic and failure analysis of composites), which was developed from a program written by Bahei-El-Din et al. (refs. 8 and 9). PAFAC uses an eight-noded hexahedral element and the least-squares method to compute the element strain components from the total of 28 strain-displacement relationships associated with all possible combinations of the eight vertices taken two at a time. Each hexahedral element represents a unidirectional composite material whose fibers are arbitrarily oriented in the structural (Cartesian) coordinate system.

Finite-Element Model

Two typical finite-element meshes used in the PAFAC program are shown in figure 9. The mesh used for a specimen with a center slit (fig. 9(a)) consisted of about 350 eight-noded hexahedral elements with about 1500 degrees of freedom. The mesh used to model a specimen with a circular hole in the center (fig. 9(b)) consisted of about 400 eight-noded hexahedral elements with about 2000 degrees of freedom. In all cases, only one-eighth of the specimen was modeled because of symmetry. Symmetry conditions were not satisfied when only one-eighth of the laminates with ±45° plies were modeled; however, we felt that the error introduced by assuming symmetry for these cases was insignificant.

At least one layer of elements is needed for every ply angle in the laminate. For example, a $[0]_6$ laminate could be modeled by one layer of elements, while a

$[\pm 45]_{2s}$ laminate would require at least two layers of elements. A uniform stress was applied to the end of the specimen to simulate the loading.

To evaluate the accuracy of the model used, the finite-element results obtained using the mesh shown in figure 9(b) for an isotropic material were compared with the exact solution for a hole in an isotropic plate corrected for finite width. For the axial stress at the edge of the hole, the two solutions differed by less than 4 percent.

Material Model

The PAFAC program uses a continuum material model developed by Bahei-El-Din and Dvorak (refs. 9 through 11) to represent the essential aspects of the elastic-plastic behavior of composite laminates. The material model is briefly described in this section.

The model consists of an elastic-plastic matrix unidirectionally reinforced by continuous elastic fibers. Both constituents are assumed to be homogeneous and isotropic. The fibers are assumed to have a very small diameter, so that although the fibers occupy a finite volume fraction of the composite, they do not interfere with matrix deformation in the two transverse directions, but only in the axial (fiber) direction. Figure 10(a) shows a schematic of this lamina model. It can also be represented by parallel fiber and matrix bars or plates with axial coupling, as illustrated in figure 10(b). In figure 10, the fiber (axial) direction is parallel to the $\bar{x}_3$-axis, and the $\bar{x}_1$- and $\bar{x}_2$-axes represent the transverse directions.

If the Cartesian coordinates are chosen so that x_3 coincides with the fiber direction, the second-order tensors of the independent stress and strain components, σ and ε, are expressed as

$$\sigma = [\sigma_{11} \ \sigma_{22} \ \sigma_{33} \ \sigma_{12} \ \sigma_{13} \ \sigma_{23}]^T$$

$$\varepsilon = [\varepsilon_{11} \ \varepsilon_{22} \ \varepsilon_{33} \ \gamma_{12} \ \gamma_{13} \ \gamma_{23}]^T$$

where $\gamma_{ij} = 2\varepsilon_{ij}$ $(i,j = 1, 2, 3; \ i \neq j)$ are the engineering shear strain components.

For equilibrium and compatibility, several requirements are imposed on the material model shown in figure 10. The stress average in each constituent can be related to the overall composite stress $\bar{\sigma}$ in the axial (fiber) direction as follows:

$$\bar{\sigma}_{33} = v_f(\sigma_{33})_f + v_m(\sigma_{33})_m \qquad (1)$$

A bar over a symbol indicates overall composite stress or strain, and the subscripts f and m denote quantities related to the fiber and matrix. The volume fractions v_f and v_m are such that $v_f + v_m = 1$. The other stress components in each constituent were assumed to be uniform and to obey the following equilibrium equations:

$$\left.\begin{aligned} \bar{\sigma}_{11} &= (\sigma_{11})_f = (\sigma_{11})_m \\ \bar{\sigma}_{22} &= (\sigma_{22})_f = (\sigma_{22})_m \\ \bar{\sigma}_{12} &= (\sigma_{12})_f = (\sigma_{12})_m \\ \bar{\sigma}_{13} &= (\sigma_{13})_f = (\sigma_{13})_m \\ \bar{\sigma}_{23} &= (\sigma_{23})_f = (\sigma_{23})_m \end{aligned}\right\} \tag{2}$$

The only constraint in the model is in the axial (fiber) direction; the matrix and fiber must deform equally. Thus,

$$\bar{\varepsilon}_{33} = (\varepsilon_{33})_f = (\varepsilon_{33})_m \tag{3}$$

The other strain components can be related to the overall strain $\bar{\varepsilon}$ as follows:

$$\bar{\varepsilon}_{ij} = v_f(\varepsilon_{ij})_f + v_m(\varepsilon_{ij})_m \qquad (ij \neq 33) \tag{4}$$

Since the fibers are elastic up to failure, the inelastic strains of the lamina are caused by matrix deformation. Because the fiber imposes an elastic constraint on the matrix which affects the shape of the lamina yield surface, additional kinematic components appear in the hardening rule of the lamina and influence the magnitude of the overall plastic strains. All aspects of the yield behavior were examined and accounted for in the formulation of the lamina constitutive equations. These equations are explicitly described in references 9 and 11.

Elastic-Plastic Response

The material model described above was used to characterize the elastic-plastic behavior of simple composite laminates. The stress-strain curve of the matrix material was modeled with a Ramberg-Osgood equation (ref. 12). In addition, the program PAFAC is able to calculate the fiber stress in each element and to model fiber breakage.

The yield pattern of the matrix material can be determined with the PAFAC model. Figure 11 shows the extent of yielded elements for increasing levels of stress applied to a $[0]_6$ laminate with a 25.4-mm-diameter hole and $2a/w = 0.25$. Only one-quarter of the specimen is shown in the figure. The sketches show the growth of yielding as applied stress is increased. The first yielding occurred at

a stress of 34 MPa, shown in figure 11(a). At the applied stress of 125 MPa, most of the specimen had yielded; only a small portion of the model above the hole remained elastic. Although not shown in the figure, the entire specimen had yielded at a stress of 275 MPa. For this example, the test results showed that fibers began to fail at about 260 MPa and the specimen failed at a stress of 540 MPa. Widespread yielding occurred before fibers broke or the specimen failed. This yielding influenced the ultimate fracture behavior of the composite. This example emphasizes the necessity for a model that can predict the elastic-plastic nonlinear behavior of the matrix phase and the elastic linear behavior of the fiber phase for metal matrix composites.

This technique can be applied to each layer of laminates with plies at different angles. Figure 12 shows the yield pattern for a $[0/\pm45]_s$ laminate with a 25.4-mm-diameter hole and $2a/w = 0.25$. The sketches show the extent of the yielding in the 0° and 45° layers as the applied stress is increased. The yielding in the -45° layer is very similar to the pattern shown for the 45° layer. The ±45° layers yielded much earlier in the loading history than the 0° layer. Although not shown in the figure, the entire specimen (all layers) had yielded at 150 MPa. As in the previous example, widespread yielding occurred before fibers broke or the specimen failed.

ANALYSIS OF FAILURE

The following equation was incorporated into the PAFAC program as the fiber failure criterion:

$$\left(\frac{\sigma_{33}^{f}}{\sigma_{33}^{ult}}\right)^2 + \left(\frac{\sigma_{13}^{f}}{\sigma_{13}^{ult}}\right)^2 \geq 1 \tag{5}$$

In this equation, σ_{33}^{f} represents the current tensile stress in the fiber and σ_{13}^{f} represents the current shear stress in the fiber. The ultimate strengths of the fiber in the tensile and shear modes are σ_{33}^{ult} and σ_{13}^{ult}, respectively. For the meshes used, the element at the notch tip was approximately three fibers wide. A mesh fine enough to model a fiber width by one element width would be prohibitively expensive. Therefore, an averaging technique was used to determine the ultimate strengths, σ_{33}^{ult} and σ_{13}^{ult} of the fibers within one element.

Since these two stengths were unknown, two test cases were required. The monolayer with a slit and a $[\pm45]_{2s}$ specimen containing a hole were selected. These two layups were chosen because for the monolayer the dominant fiber stress at the crack tip was the tensile stress σ_{33}^{f}, while in the $[\pm45]_{2s}$ laminate the dominant fiber stress was the shear stress σ_{13}^{f}. From the radiographs, the laminate stress at first fiber failure could be closely estimated. The finite-element model for each laminate configuration was loaded to the approximate stress when first fiber failure occurred. The corresponding fiber stresses σ_{33}^{f} and σ_{13}^{f} were recorded for the element where first fiber failure was observed. The pairs of values for σ_{33}^{f} and σ_{13}^{f} for both the $[\pm45]_{2s}$ and monolayer specimens were substituted in equation (5). The two equations were then solved for the two unknowns, σ_{33}^{ult} and σ_{13}^{ult}. This gave the values of 2300 MPa and 270 MPa, respectively. First fiber failure was predicted for the other laminates using these values.

To validate this method of determining element fiber strengths, these values were used in the finite-element model to study the fiber stress in the region of notches. For the unidirectional monolayer with a center slit, figure 13 shows how the fiber stress varies in the region of the crack tip. The solid line represents data results from the finite-element analysis. The program predicts stresses only at element centroids; therefore, to obtain the stress in the first fiber, it was necessary to extrapolate the stress from the element centroid to the edge of the notch. This extrapolation is represented by the dashed line in figure 13. As indicated in the figure, the crack-tip element contained approximately 2.3 fibers. The ultimate strength of a single fiber was assumed to be 3160 MPa, which was obtained from tensile tests of unnotched 0° B/Al specimens (ref. 5). The stress at the center of the fiber next to the crack tip was 3160 MPa when the applied remote stress was 262.5 MPa, a reasonable estimate of the remote stress at first fiber failure. The corresponding stress at the center of the element next to the crack tip was found to be about 2300 MPa. Figure 14 shows a similar plot of the fiber stress concentration for a $[0]_6$ laminate with a hole. In this example, the element next to the hole contained approximately 3.6 fibers. Here the stress at the center of the fiber next to the hole was found to be about 3160 MPa when the applied remote stress was 465 MPa. Again, the stress at the center of the element next to the hole was about 2300 MPa.

At each incremental load level, the program checked the state of fiber stresses in each element. When equation (5) was satisfied, the fibers of that element were broken. In the PAFAC program, it is possible to continue the analysis after first fiber failure. However, because of the inability of the program to model element unloading when a fiber broke, we felt that for this study, any calculations made after first fiber failure would be unrealistic; therefore, the analysis was terminated at the point of first fiber failure.

COMPARISON OF PREDICTED AND EXPERIMENTAL RESULTS

In this section, the predicted mechanical behavior of notched B/Al composite specimens is compared with actual test data. To show the capability of the analysis to predict small-scale, localized mechanical behavior, crack-opening displacements (COD) were predicted for the specimens containing slits tested by Awerbuch and Hahn (ref. 4). The data of reference 4, which were the only COD data available for comparison, were for unidirectional specimens. A plot of the specimen applied load versus the measured and predicted COD is shown in figure 15. The PAFAC model predicted COD very accurately up to first fiber failure.

As discussed earlier, the finite-element program PAFAC can predict first fiber failure around a notch. The first fiber is assumed to fail when the fiber stresses within an element exceed the criterion given in equation (5). As previously explained, the elements near the notch tip were approximately three fibers wide. Therefore, "first fiber failure" actually indicated failure of all three fibers within an element. The following sections show the correlation between the predicted first fiber failure and the observed first fiber failure for several different laminates containing both holes and slits. Ultimate strength data are also presented.

Specimens With Holes

In figure 16 the applied laminate stress is plotted against the specimen overall strain for a unidirectional specimen containing a circular hole. The solid line

represents the predicted response up to first fiber failure. There is excellent correlation between the predicted and observed results up to first fiber failure. As previously noted, the first fiber failed quite early in the loading history for the unidirectional specimens. The sketch shows the predicted location of the first fiber failure.

Figure 17 shows the predicted curve and experimental results for two $[\pm 45]_{2s}$ specimens. There was considerable scatter in the data. The predicted curve lies just above the upper experimental curve, for which the stress at first fiber failure is expected to be near the laminate failure stress, as observed in the lower curve.

The results for a $[0/\pm 45]_s$ laminate are shown in figure 18. Again, there is a very good correlation between the predicted and the experimental stress-strain behavior. First fiber failure was predicted to occur near laminate failure. Recall that first fiber failure was not observed for this laminate and therefore was assumed to occur at laminate failure. The first fiber failure was predicted next to the hole in the 0° ply element on the transverse axis, as shown by the sketch. Figure 19 shows similar results for a $[0_2/\pm 45]_s$ laminate. This layup was more dominated by 0° fibers than the $[0/\pm 45]_s$ laminate, so less plasticity was predicted.

Specimens With Slits

The PAFAC analysis was also used to predict first fiber failure of a unidirectional monolayer containing a crack-like slit. The results are shown in figure 20. The yield pattern that developed at the notch tip (fig. 20(a)) extends perpendicular to the notch, parallel to the fibers. This behavior has been observed by Jones (ref. 6). Figure 20(b) presents a plot of the normalized fiber stress (fiber failure criterion) versus laminate stress. The solid line represents the predicted fiber stress up to first fiber failure. The dashed line shows the laminate stress for which the first fiber failure was observed. Again, the predicted and observed laminate stresses at first fiber failure agree very well.

Several specimens containing crack-like slits tested by Poe and Sova (ref. 1) were also analyzed with the PAFAC program. Figure 21 shows the predicted and experimental results for a 51-mm-wide $[0]_6$ specimen containing a 15-mm slit. Poe and Sova measured the remote strain with strain gages. The predicted strains at the same location are compared in figure 21 with the measured remote strains. Again, as with all the other unidirectional specimens tested, the first fiber is predicted to fail early in the loading history. Poe and Sova observed this early failure of fibers but did not record the stress at which the fibers began to fail. The stress-strain prediction is quite good.

Figure 22 shows similar analytical and experimental results (ref. 1) for a 102-mm-wide $[0/\pm 45]_s$ specimen containing a 10-mm slit. The PAFAC model predicted stress-strain response very well. The predicted first fiber failure was very close to the laminate failure stress.

Summary of Analytical Predictions

The PAFAC model produces very good predictions of observed mechanical behavior of B/Al composite specimens containing either circular holes or crack-like slits. The model accurately predicts stress-strain responses of the notched composites, including widespread yielding, and can predict first fiber failure. Because first

fiber failure occurs very close to overall laminate failure in all laminates examined except the unidirectional ones, the first fiber failure criterion is sufficient for predicting ultimate strength of most laminates containing notches. Figures 23 and 24 summarize the elastic-plastic strength predictions made with the first fiber failure criterion. The predictions were made on specimens of various widths and ratios of notch length to specimen width (2a/w), as noted in the figures.

CONCLUSIONS

Metal matrix composites in general, boron/aluminum composites in particular, are subject to widespread yielding. This plasticity complicates the analysis of metal matrix composites containing notches. This report presented experimental results for five laminate orientations of boron/aluminum composites containing circular holes and crack-like slits. Specimen stress-strain behavior, stress at first fiber failure, and ultimate strength were determined from tests. The specimens were then analyzed with a three-dimensional elastic-plastic finite-element program. Predicted mechanical behavior was compared with test results. The following conclusions were derived from this work:

1. For notched $[\pm 45]_{2s}$, $[0/\pm 45]_{s}$, and $[0_2/\pm 45]_{s}$ specimens, the first fibers failed at a stress level near the specimen ultimate strength.

2. For notched unidirectional laminate specimens, the first fiber failure occurred at approximately one-half of the specimen ultimate strength.

3. Acoustic emissions were useful for monitoring fiber breaks in unidirectional composites, but were inconclusive for other laminate orientations.

4. Circular holes and crack-like slits of the same characteristic length produced approximately the same strength reduction.

5. Matrix plasticity had to be accounted for to accurately predict the stress-strain and failure responses of boron/aluminum composites.

6. The PAFAC model predicted stress-strain responses and stress at first fiber failure very well for laminates containing 0° plies and reasonably well for $[\pm 45]_{2s}$ laminates.

Langley Research Center
National Aeronautics and Space Administration
Hampton, VA 23665
July 8, 1983

REFERENCES

1. Poe, C. C., Jr.; and Sova, J. A.: Fracture Toughness of Boron/Aluminum Laminates With Various Proportions of 0° and ±45° Plies. NASA TP-1707, 1980.

2. Prewo, K. M.: The Notched Tensile Behavior of Metal Matrix Composites. Composite Materials: Testing and Design (Third Conference), ASTM STP 546, 1974, pp. 507-522.

3. Mar, James W.; and Lin, Kuen Y.: Fracture of Boron/Aluminum Composites With Discontinuities. J. Compos. Mater., vol. 11, Oct. 1977, pp. 405-421.

4. Awerbuch, Jonathan; and Hahn, H. Thomas: Crack-Tip Damage and Fracture Toughness of Boron/Aluminum Composites. J. Compos. Mater., vol. 13, Apr. 1979, pp. 82-107.

5. Sova, J. A.; and Poe, C. C., Jr.: Tensile Stress-Strain Behavior of Boron/Aluminum Laminates. NASA TP-1117, 1978.

6. Jones, Walter F.: Experimental Determination of Internal Damage Growth in Unidirectional Boron/Aluminum Composite Laminates. Ph.D. Disser., Clemson Univ., Aug. 1982.

7. Bigelow, C. A.; and Bahei-El-Din, Y. A.: Plastic and Failure Analysis of Composites (PAFAC). LAR-13183, COSMIC, Univ. of Georgia, 1983.

8. Bahei-El-Din, Yehia A.; Dvorak, George J.; and Utku, Senol: Finite Element Analysis of Elastic-Plastic Fibrous Composite Structures. Comput. & Struct., vol. 13, no. 1-3, June 1981, pp. 321-330.

9. Bahei-El-Din, Yehia Ahmed: Plastic Analysis of Metal-Matrix Composite Laminates. Ph.D. Disser., Duke Univ., 1979.

10. Dvorak, George J.; and Bahei-El-Din, Yehia A.: Plasticity of Composite Laminates. Research Workshop on Mechanics of Composite Materials, Duke Univ., Oct. 1978, pp. 32-54.

11. Bahei-El-Din, Y. A.; and Dvorak, G. J.: Plastic Yielding at a Circular Hole in a Laminated FP-Aℓ Plate. Modern Developments in Composite Materials and Structures, J. R. Vinson, ed., American Soc. Mech. Eng., c.1979, pp. 123-147.

12. Ramberg, Walter; and Osgood, William R.: Description of Stress-Strain Curves by Three Parameters. NACA TN 902, 1943.

TABLE I.- RATIOS OF HOLE DIAMETER TO SPECIMEN WIDTH

w, mm	Ratio 2a/w for hole diameter, 2a, mm, of -			
	3.18	6.35	12.70	25.40
51	0.0625	0.125	0.250	
102			.125	0.250

TABLE II.- TENSILE PROPERTIES OF UNNOTCHED B/Al LAMINATES

[Data from refs. 1 and 5]

Laminate orientation	w, mm	Ultimate tensile strength, MPa
$[0]_6$	19	1672
$[0_2/\pm45]_s$	19	800
$[0/\pm45]_s$	19	581
$[\pm45]_{2s}$	19	221
$[\pm45]_{2s}$	51	281
$[\pm45]_{2s}$	102	331

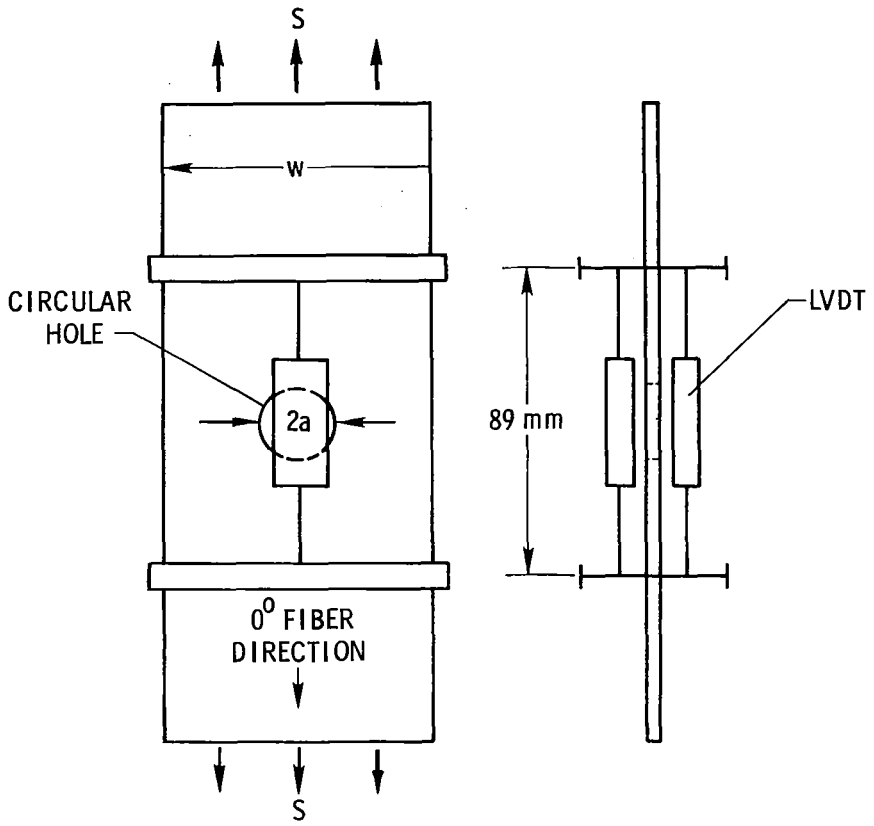

Figure 1.- Typical B/Al composite tensile specimen with linearly varying displacement transducer (LVDT) attached.

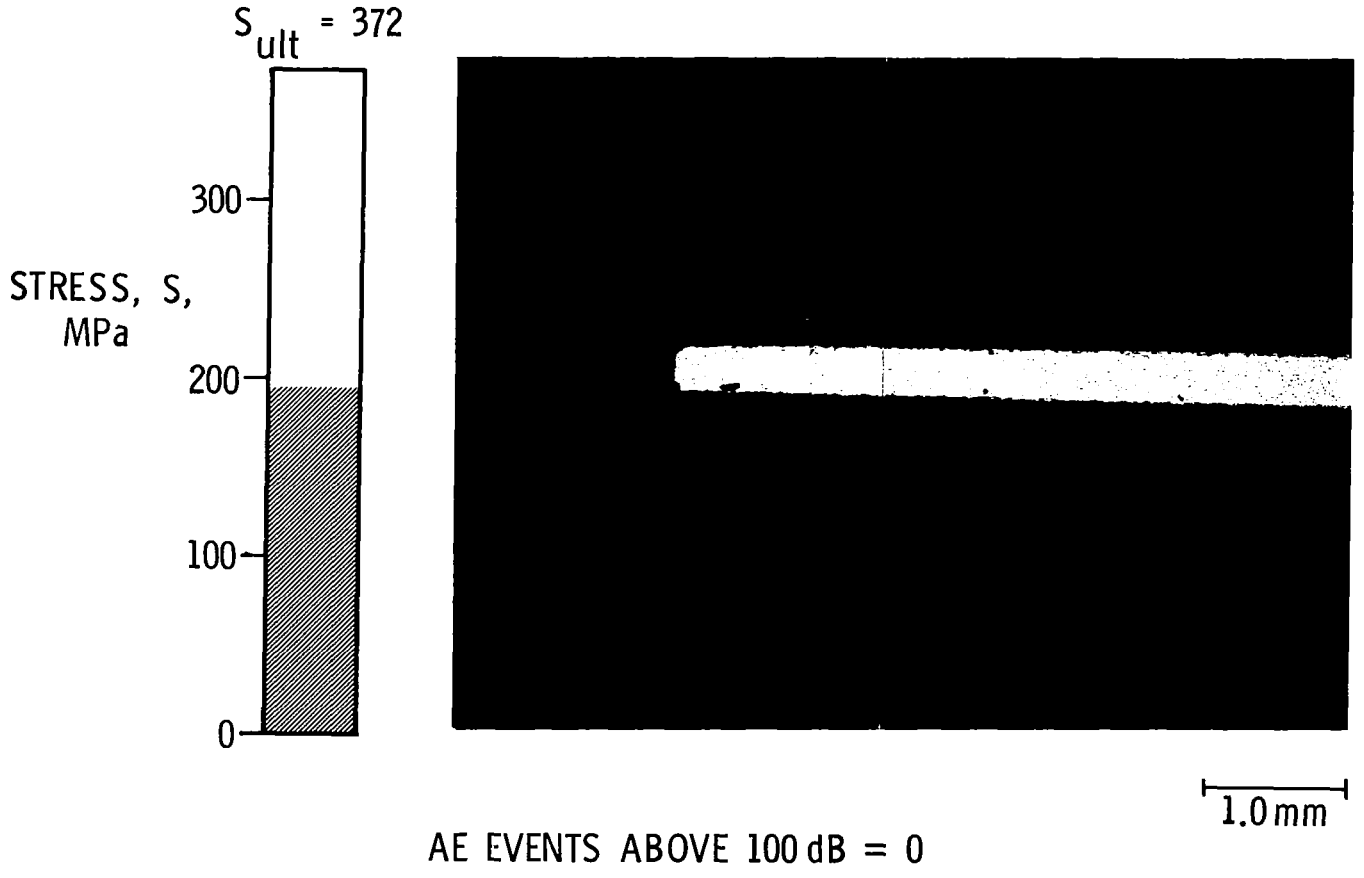

(a) No damage.

Figure 2.- Fracture process of a unidirectional monolayer containing a crack-like slit. v_f = 0.30; w = 78 mm; 2a = 19 mm. (Figure shows one end of the center slit.)

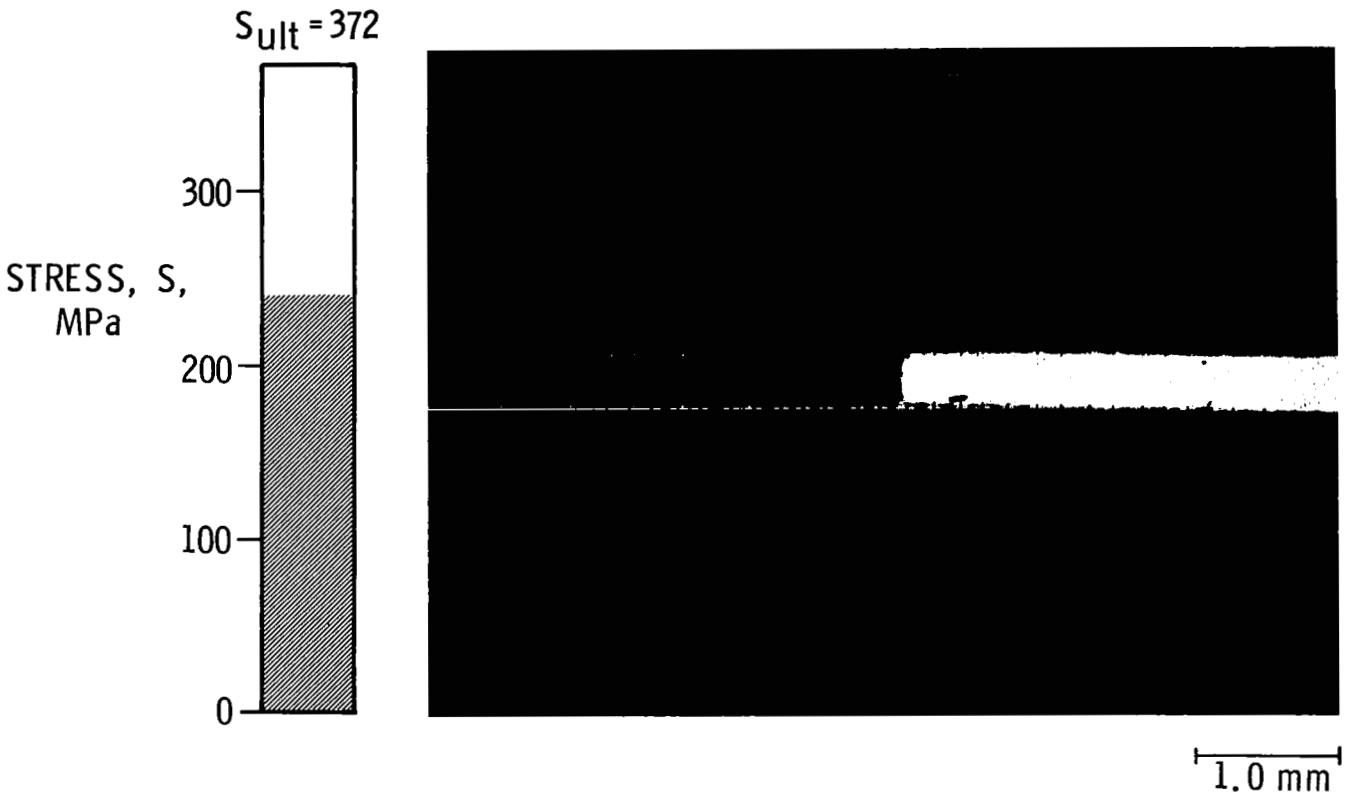

(b) Two broken fibers.

Figure 2.- Continued.

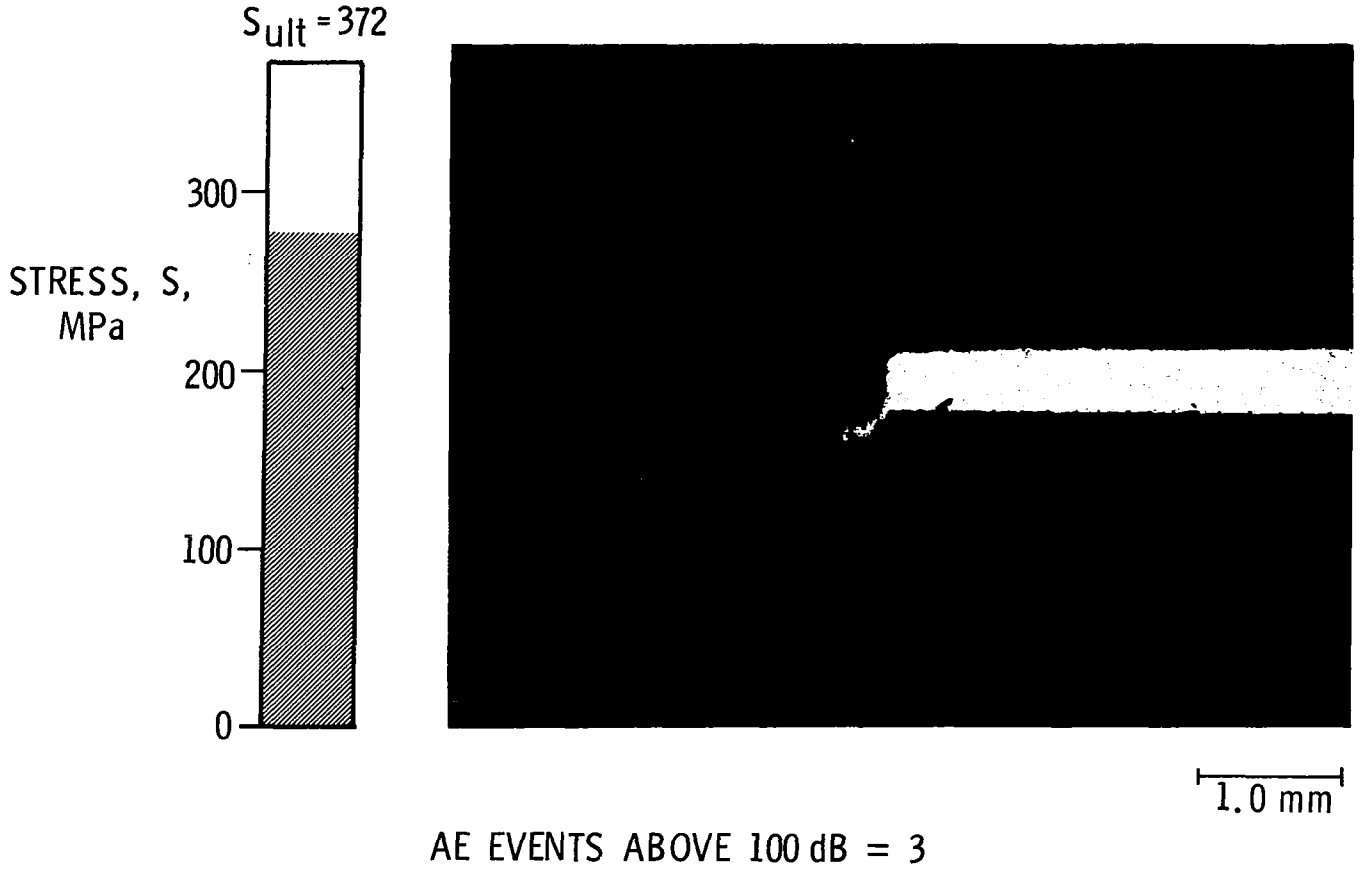

(c) Six broken fibers and matrix crack.

Figure 2.- Continued.

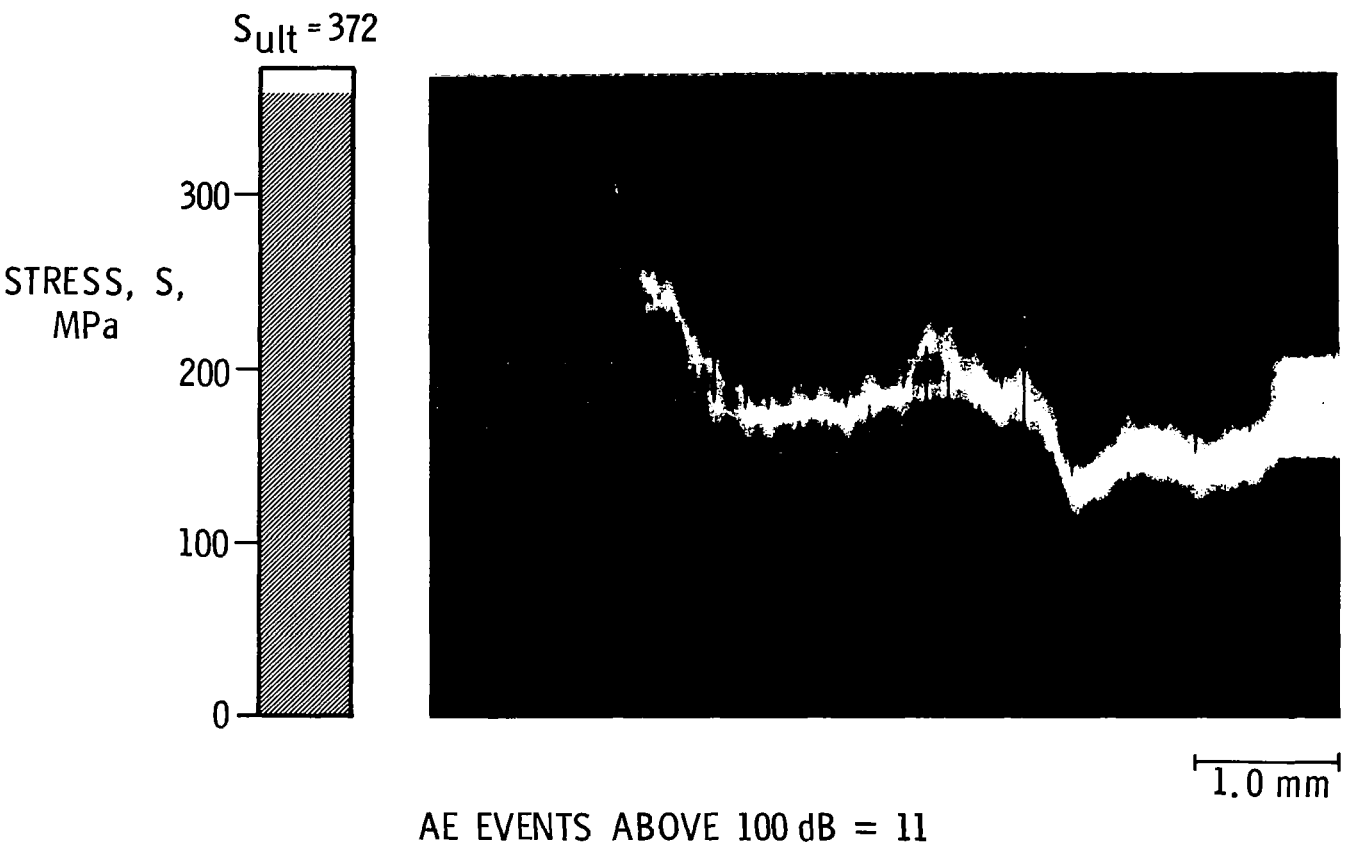

(d) Twenty-seven broken fibers and matrix crack.

Figure 2.- Concluded.

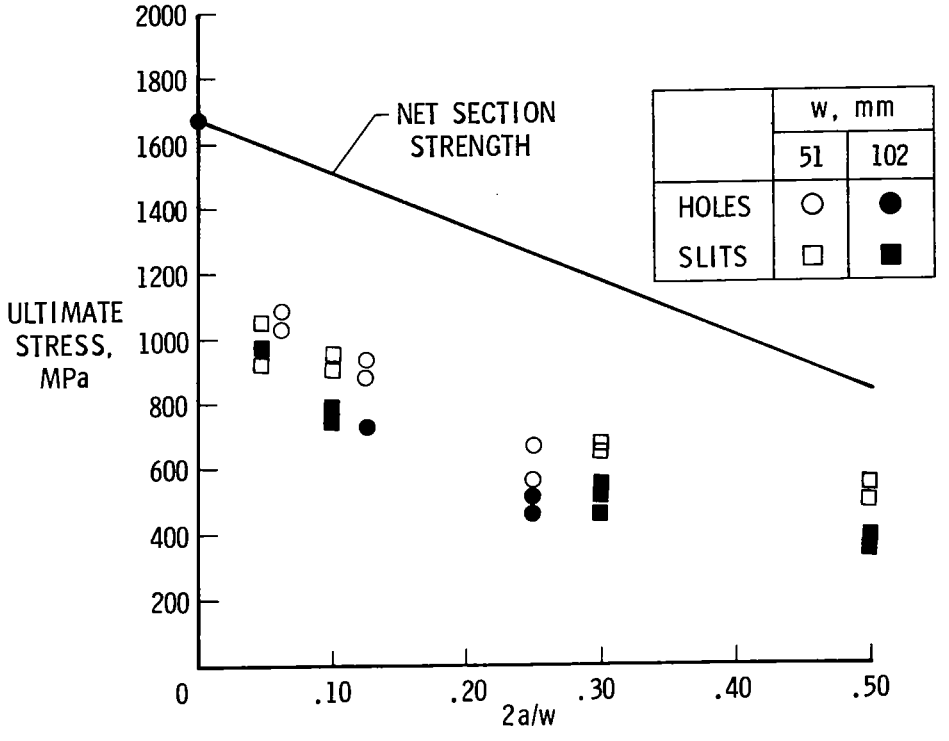

Figure 3.- Strength of $[0]_6$ laminates with holes or slits. v_f = 0.50. (Slit data from ref. 1.)

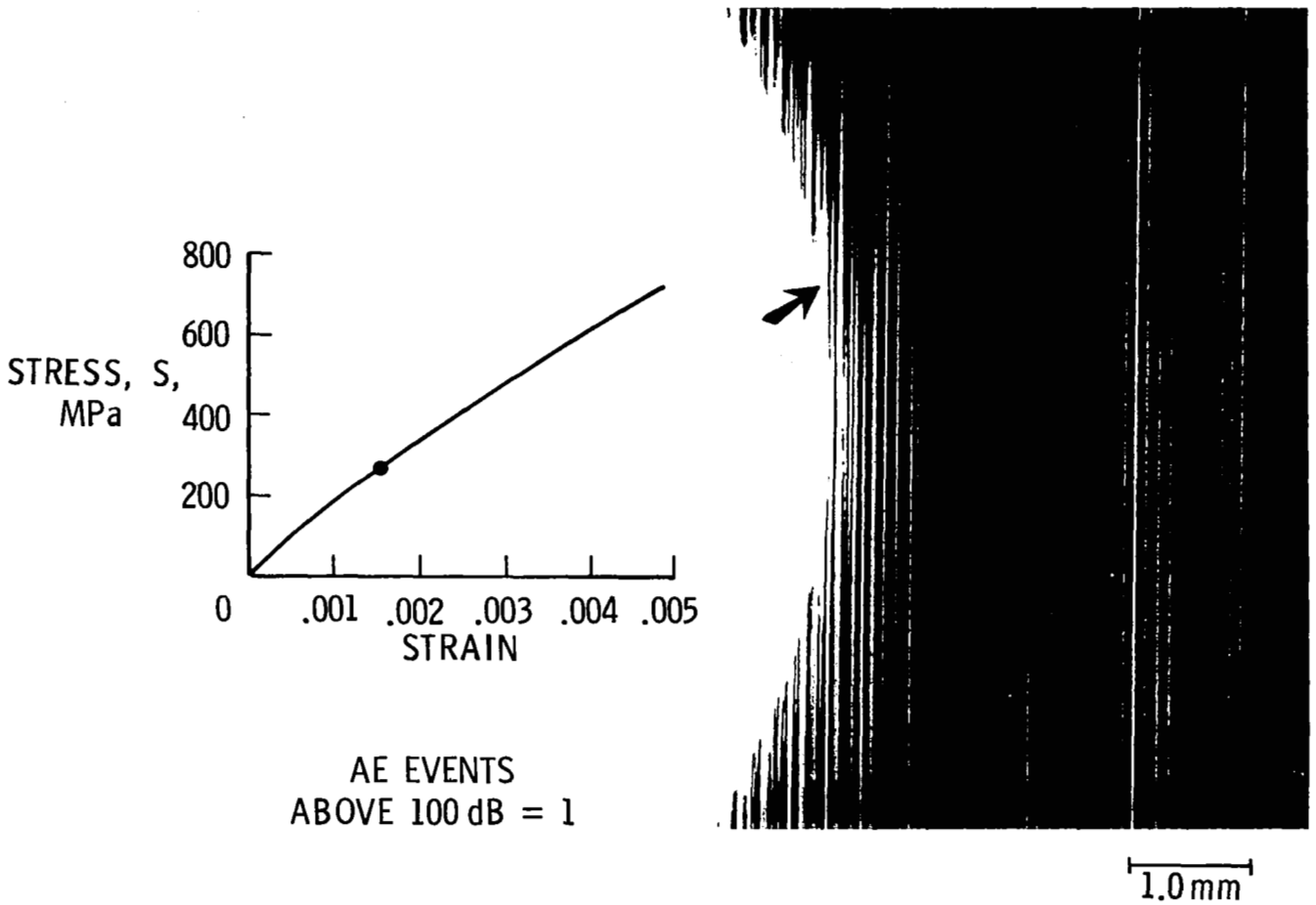

(a) First evidence of damage at 270 MPa.

Figure 4.- Fracture process of a $[0]_6$ laminate containing a circular hole. v_f = 0.50; w = 102 mm; 2a = 12.7 mm.

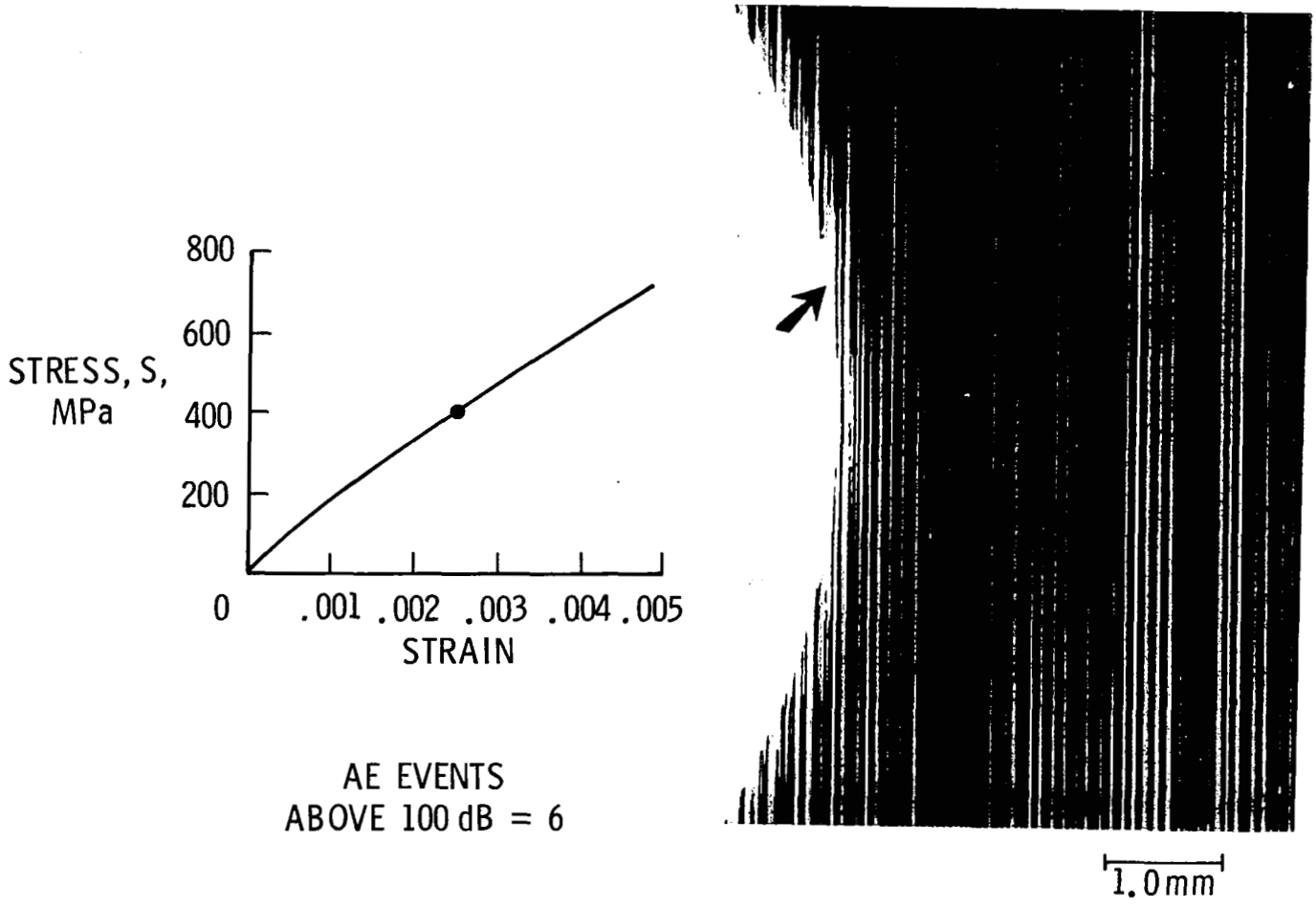

(b) Damage at 400 MPa.

Figure 4.- Continued.

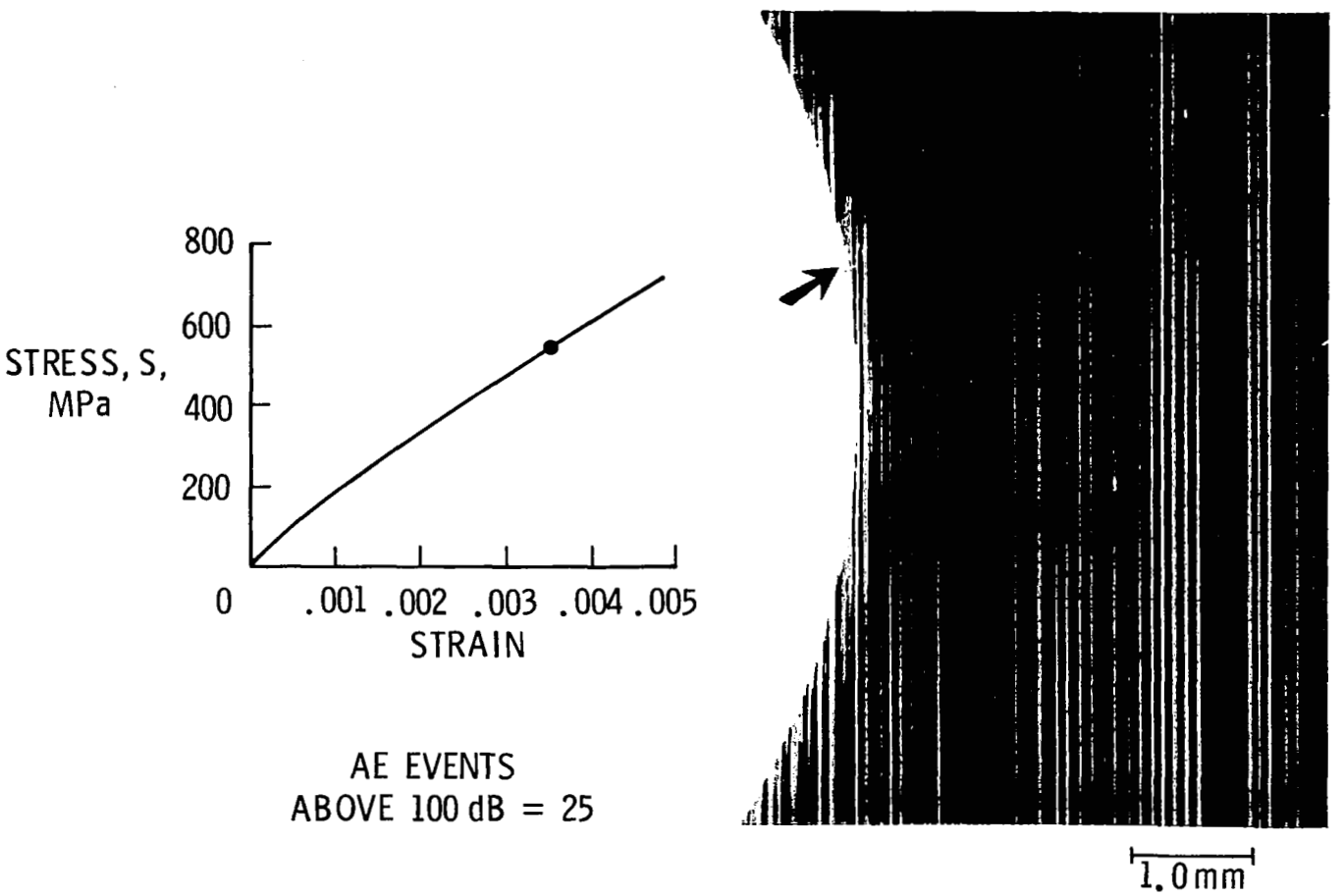

(c) Damage at 550 MPa.

Figure 4.- Continued.

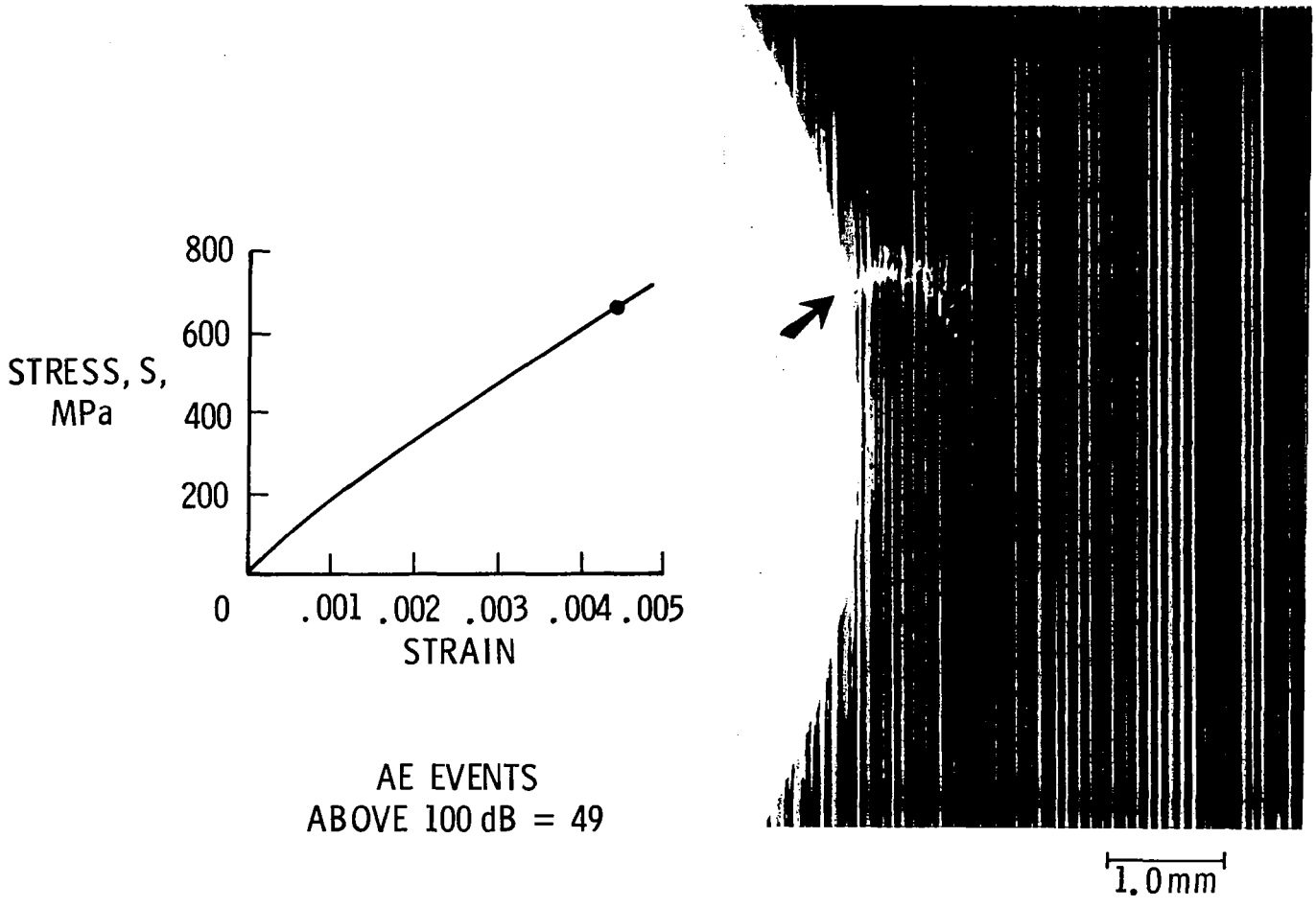

(d) Damage just before failure.

Figure 4.- Concluded.

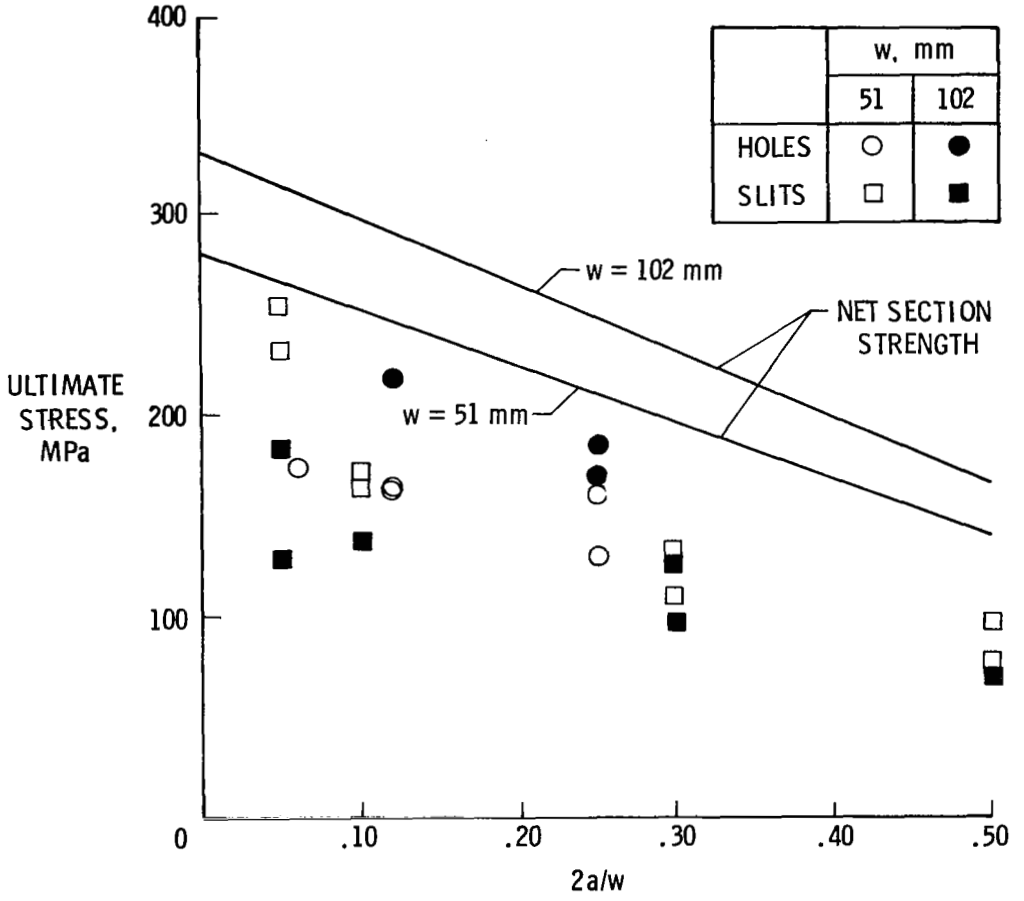

Figure 5.- Strength of $[\pm 45]_{2s}$ laminates with holes or slits. $v_f = 0.45$. (Slit data from ref. 1.)

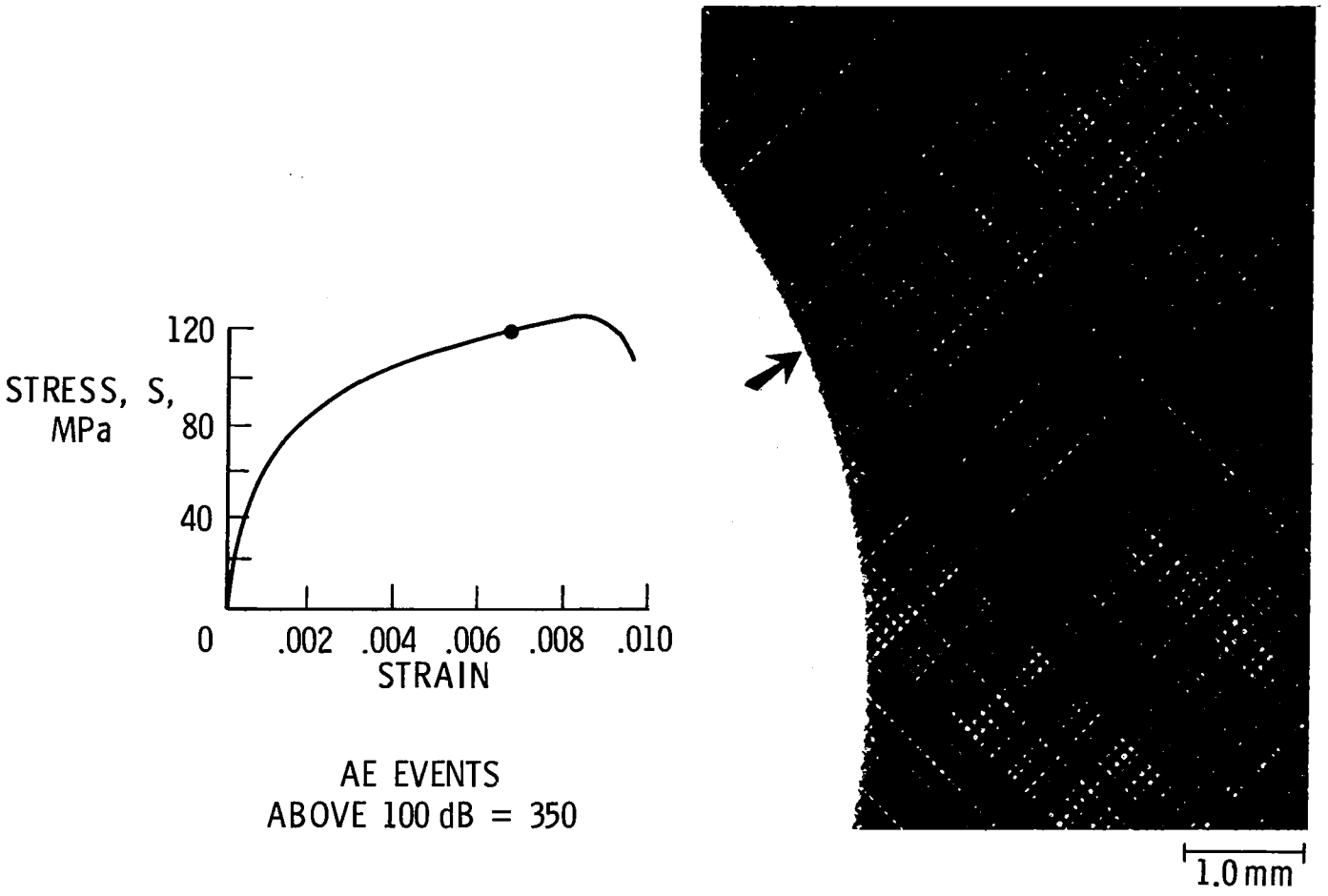

(a) First evidence of damage at 120 MPa.

Figure 6.- Fracture process of a [±45] laminate containing a circular hole. v_f = 0.45; w = 51 mm; 2a = 12.7 mm. (Test was conducted under strain control.)

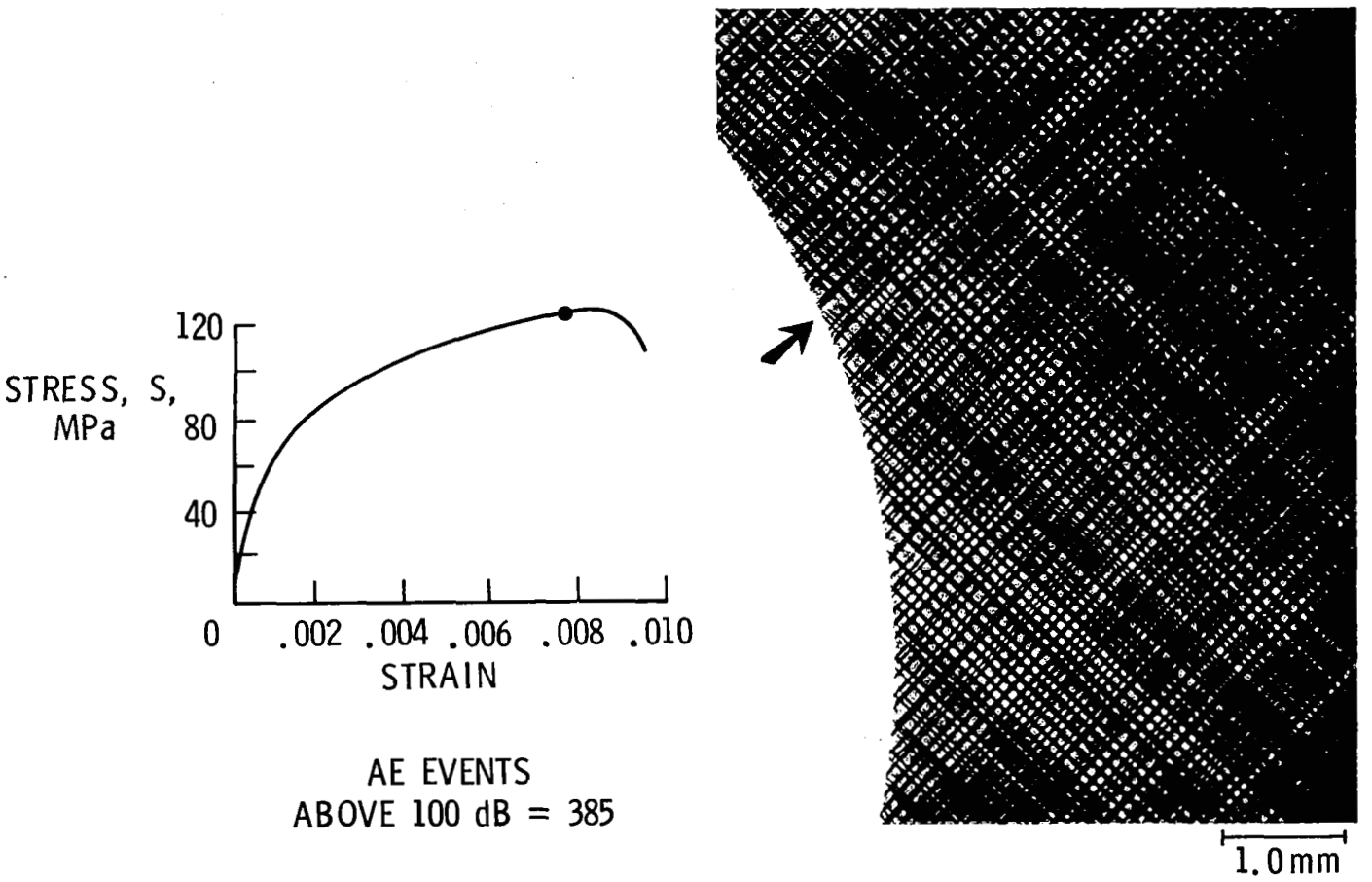

(b) Damage at 122 MPa.

Figure 6.- Continued.

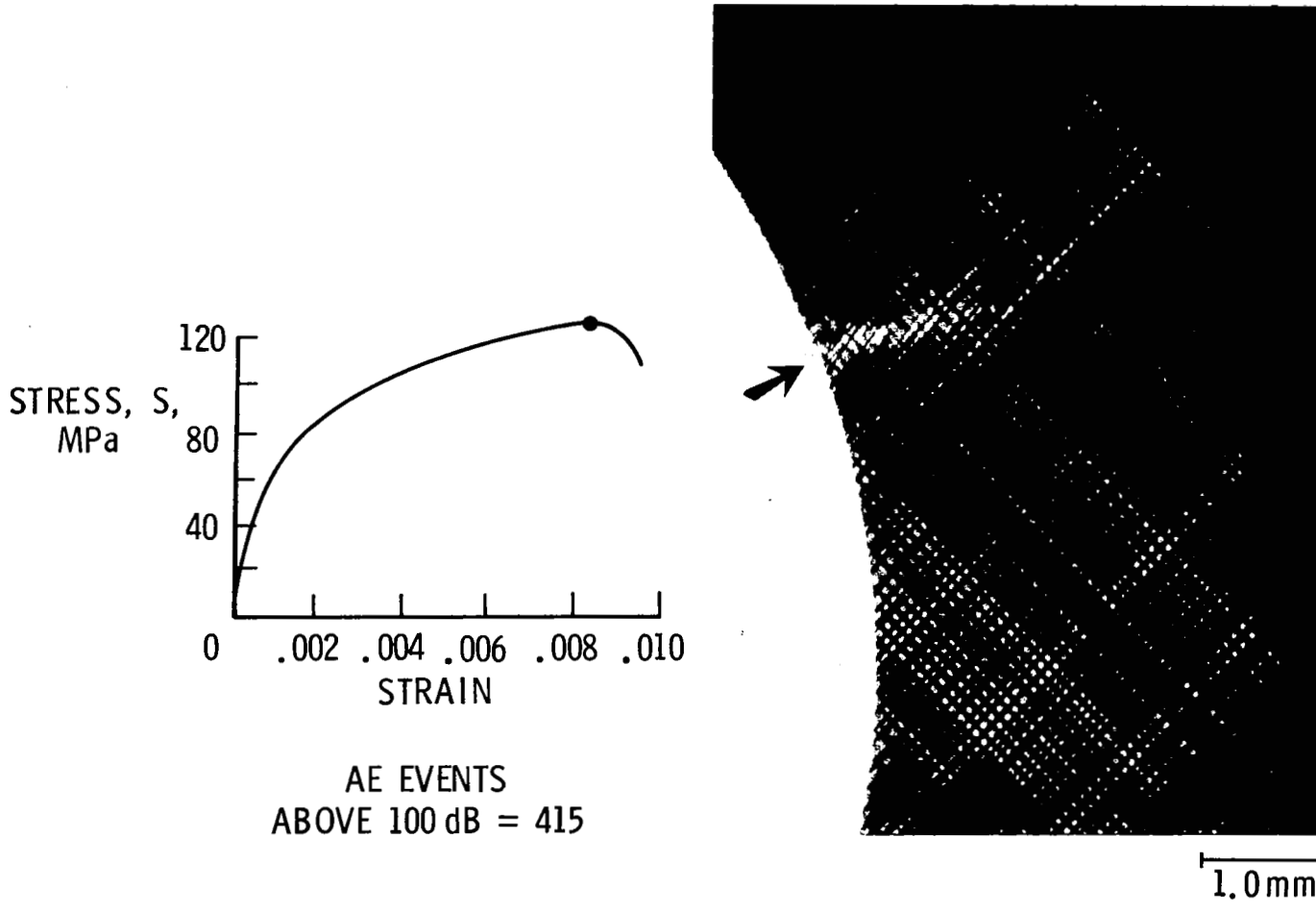

(c) Unstable damage state.

Figure 6.- Continued.

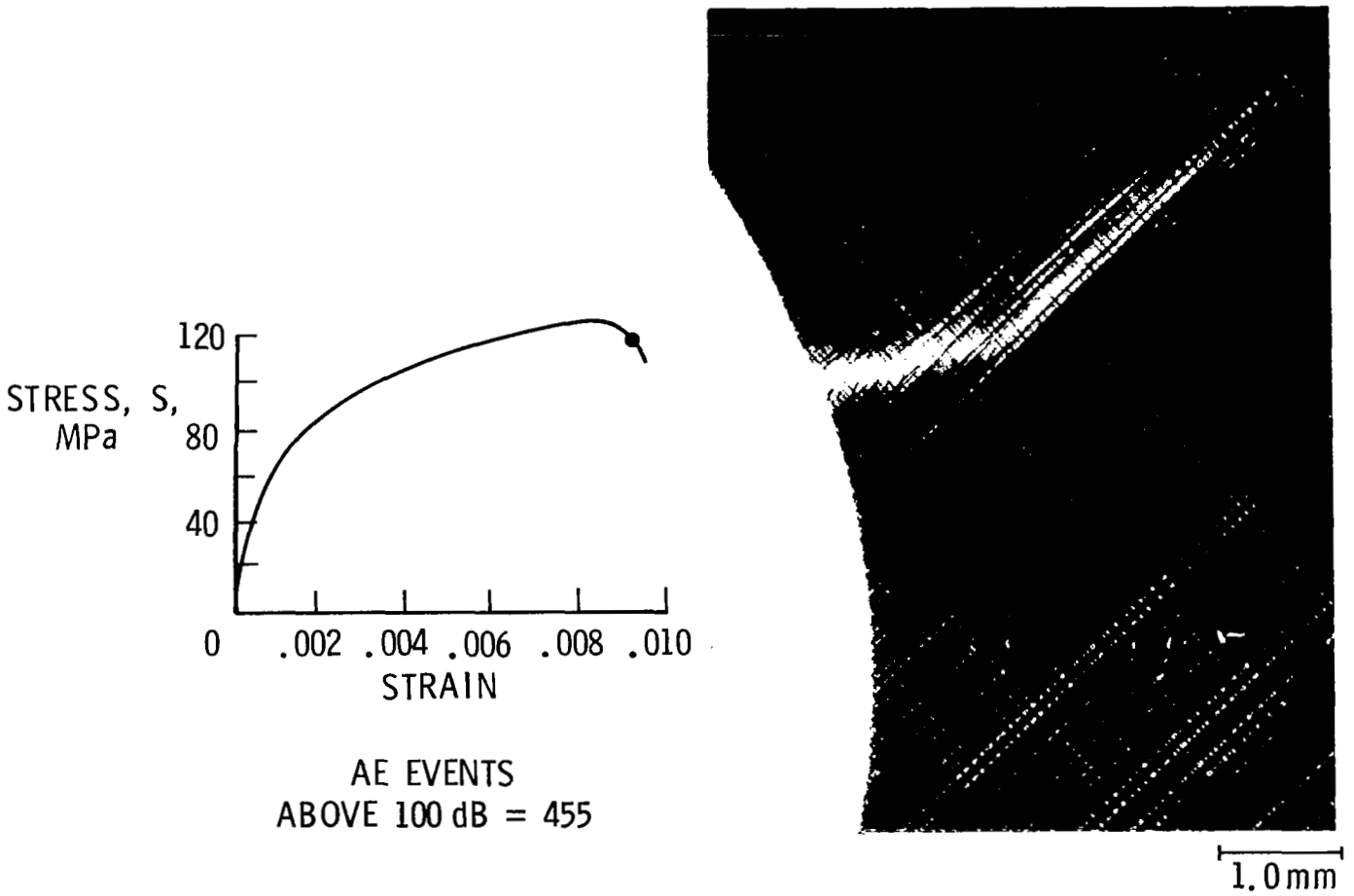

(d) Unstable damage growth.

Figure 6.- Concluded.

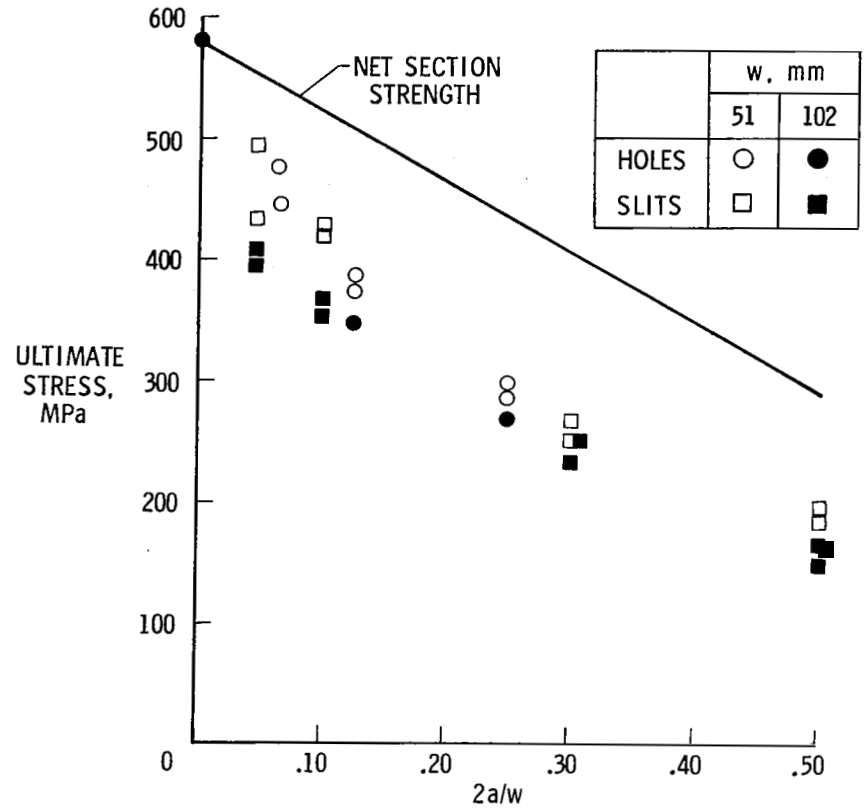

Figure 7.- Strength of $[0/\pm45]_s$ laminates with holes or slits. v_f = 0.45. (Slit data from ref. 1.)

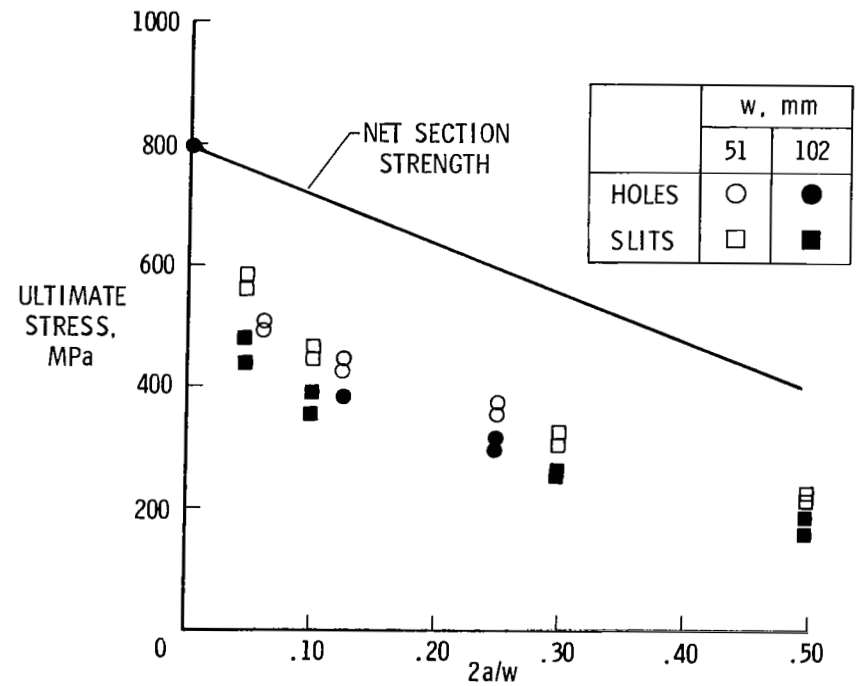

Figure 8.- Strength of $[0_2/\pm45]_s$ laminates with holes or slits. v_f = 0.45. (Slit data from ref. 1.)

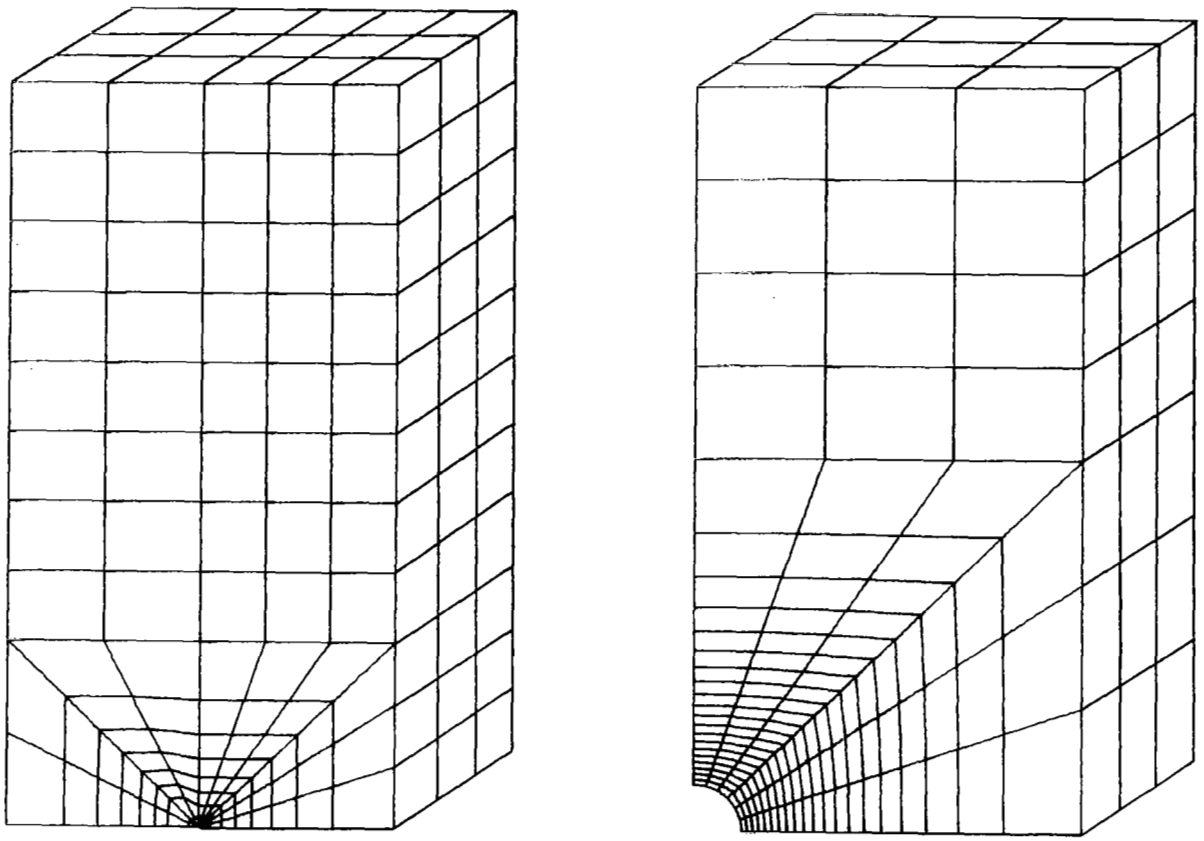

(a) Slit.

(b) Hole.

Figure 9.- Typical meshes used in finite-element analysis program.

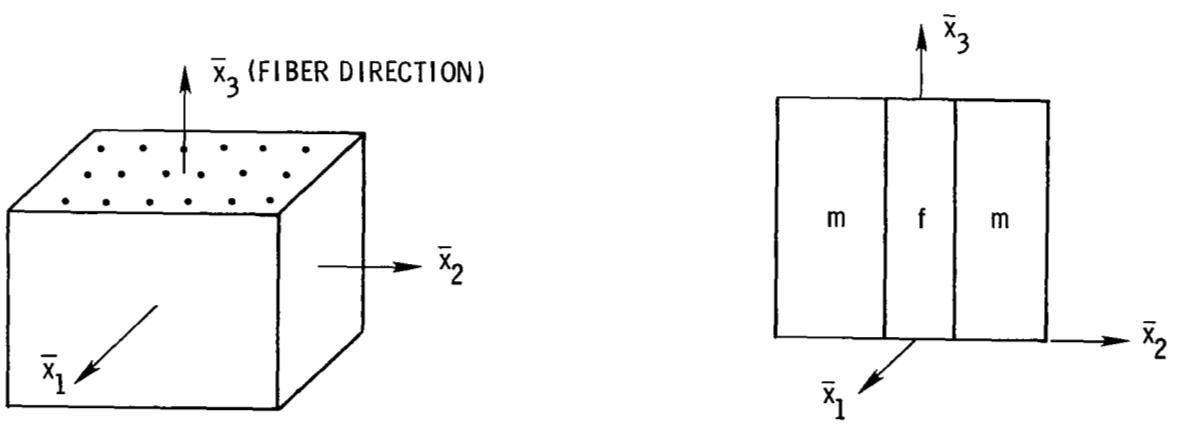

(a) Schematic model of lamina.

(b) Parallel fiber and matrix bars.

Figure 10.- Element material model.

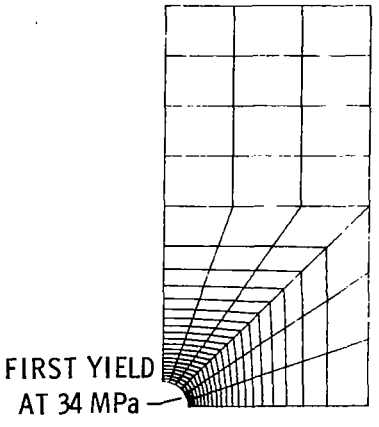

(a) S = 50 MPa.

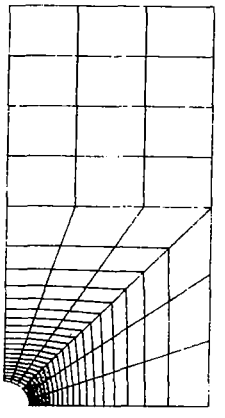

(b) S = 75 MPa.

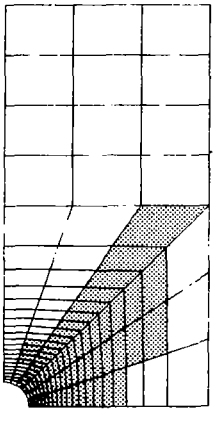

(c) S = 100 MPa.

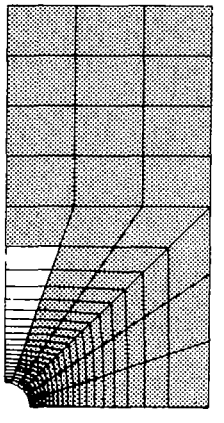

(d) S = 125 MPa.

Figure 11.- Yield pattern (shaded area) for $[0]_6$ laminate with a circular hole. 2a = 25 mm; w = 102 mm; S_{ult} = 540 MPa.

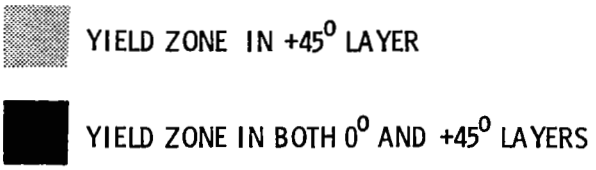

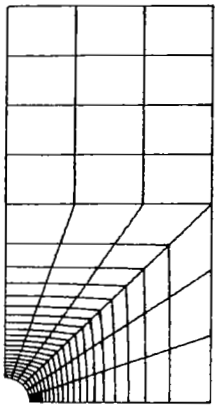

(a) S = 33.33 MPa.

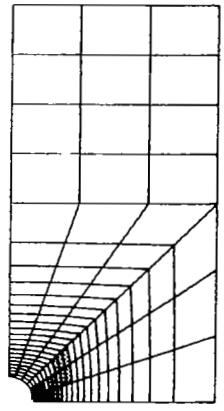

(b) S = 40.00 MPa.

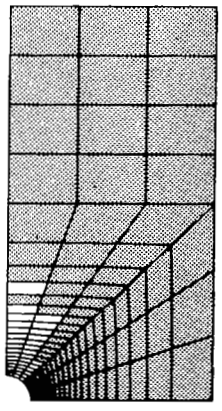

(c) S = 53.33 MPa.

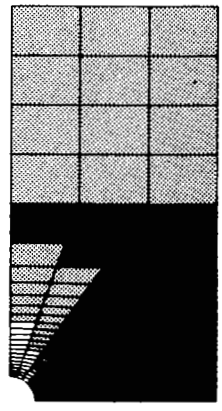

(d) S = 66.67 MPa.

Figure 12.- Yield pattern for $[0/\pm45]_s$ laminate with a circular hole. 2a = 25.4 mm; w = 102 mm; S_{ult} = 261 MPa.

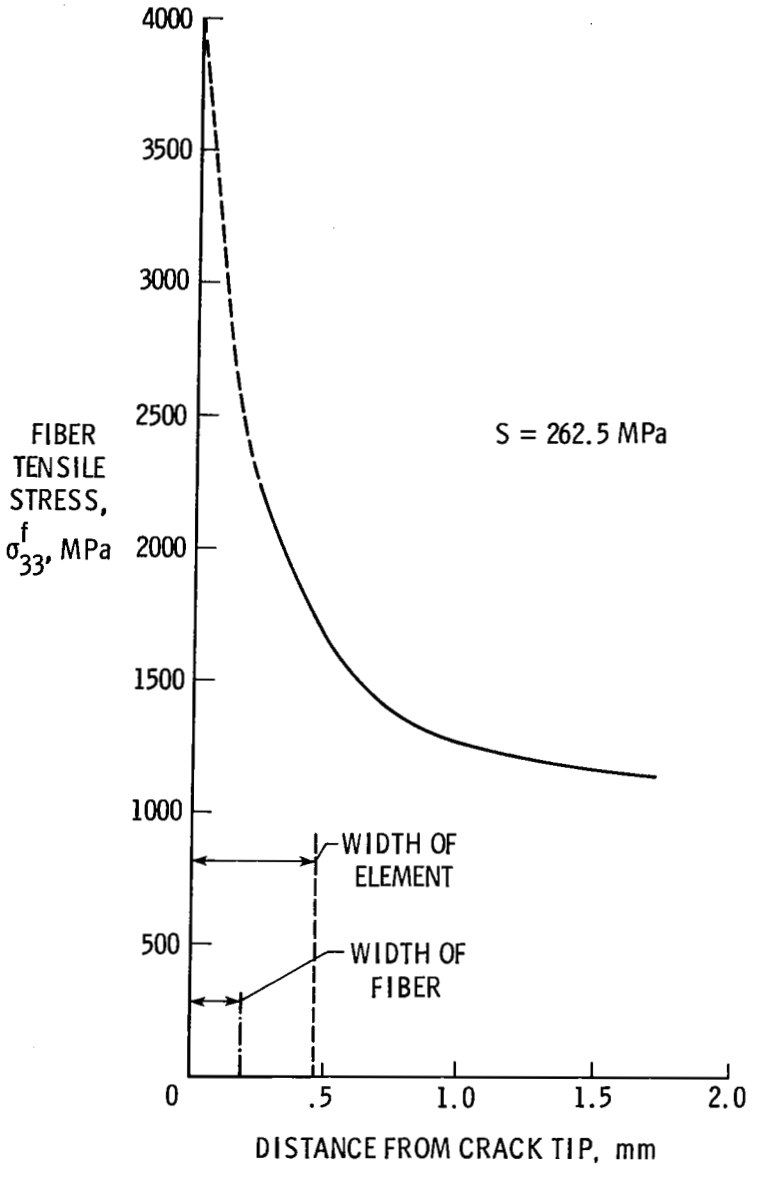

Figure 13.- Predicted fiber stress distribution near crack tip for monolayer specimen. 2a = 19 mm; w = 76 mm.

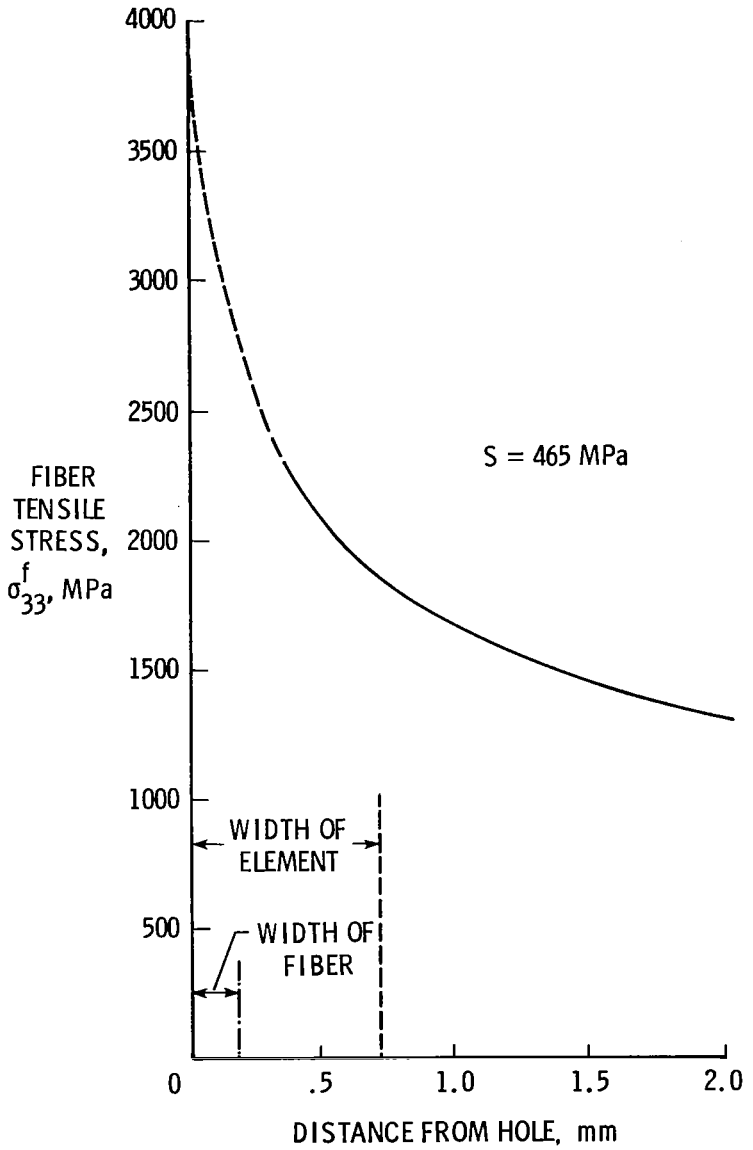

Figure 14.- Predicted fiber stress distribution near circular hole for $[0]_6$ laminate. 2a = 12.7 mm; w = 102 mm.

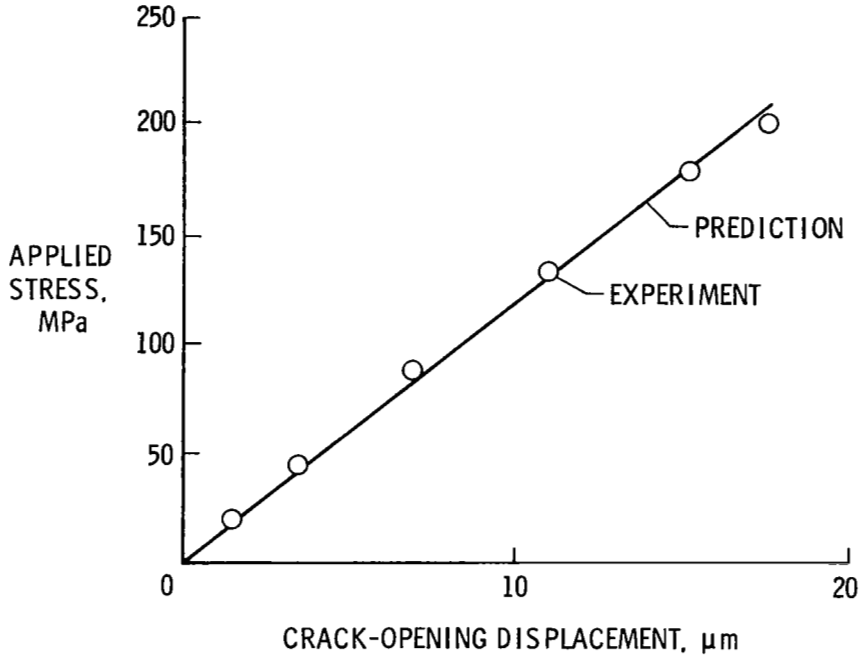

Figure 15.- Comparison of measured and predicted crack-opening displacements for 1.32-mm-thick $[0]_6$ laminate. 2a = 7.73 mm; w = 25.4 mm. (Data from ref. 4.)

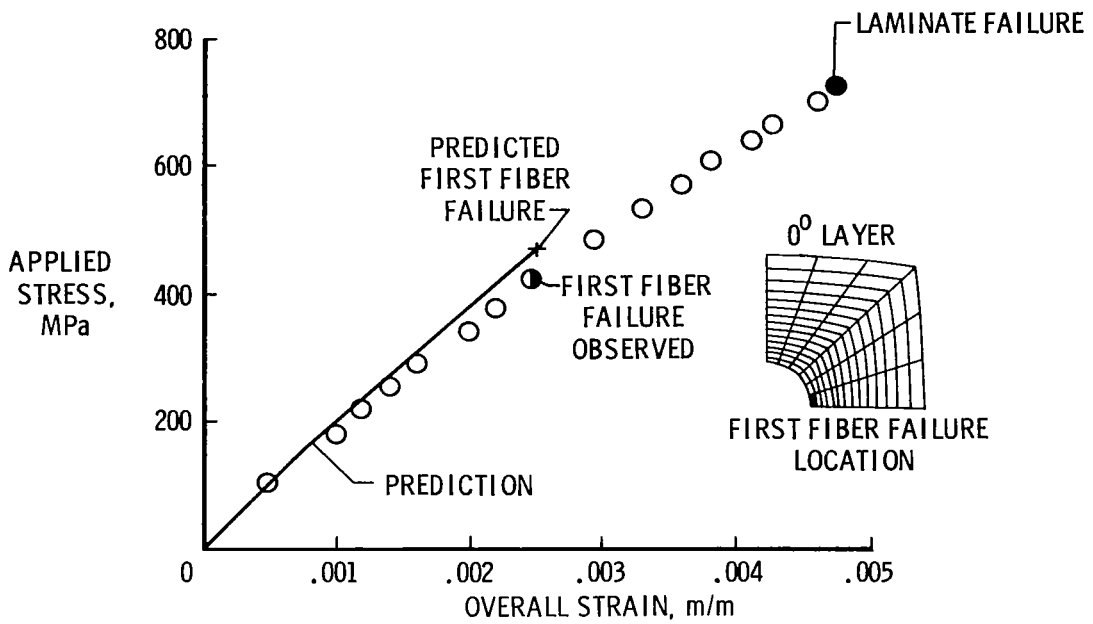

Figure 16.- Stress-strain response to failure of $[0]_6$ laminate with circular hole. 2a = 12.7 mm; w = 102 mm.

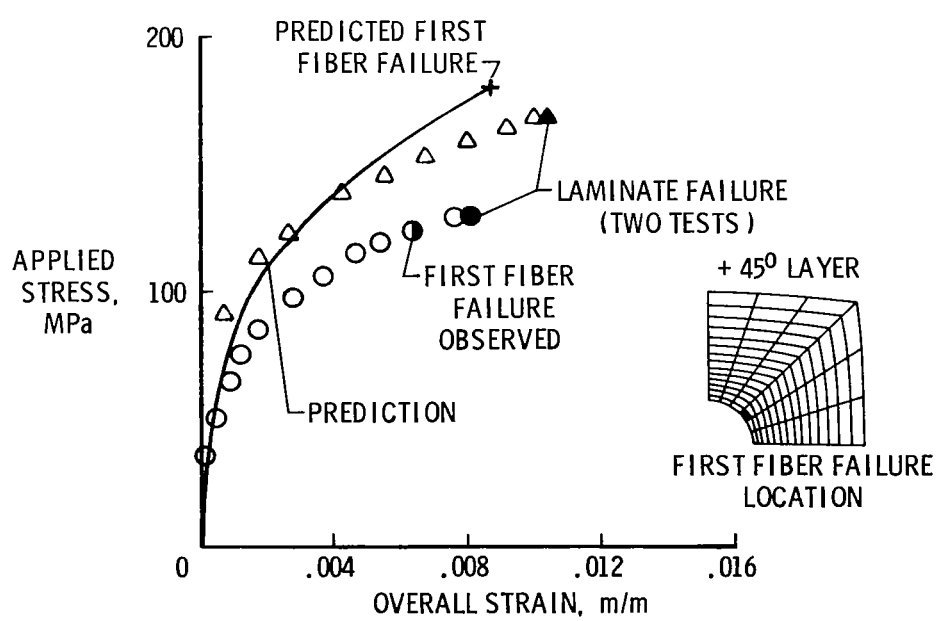

Figure 17.- Stress-strain response to failure of two $[\pm 45]_{2s}$ laminates with circular holes. 2a = 25.4 mm; w = 102 mm.

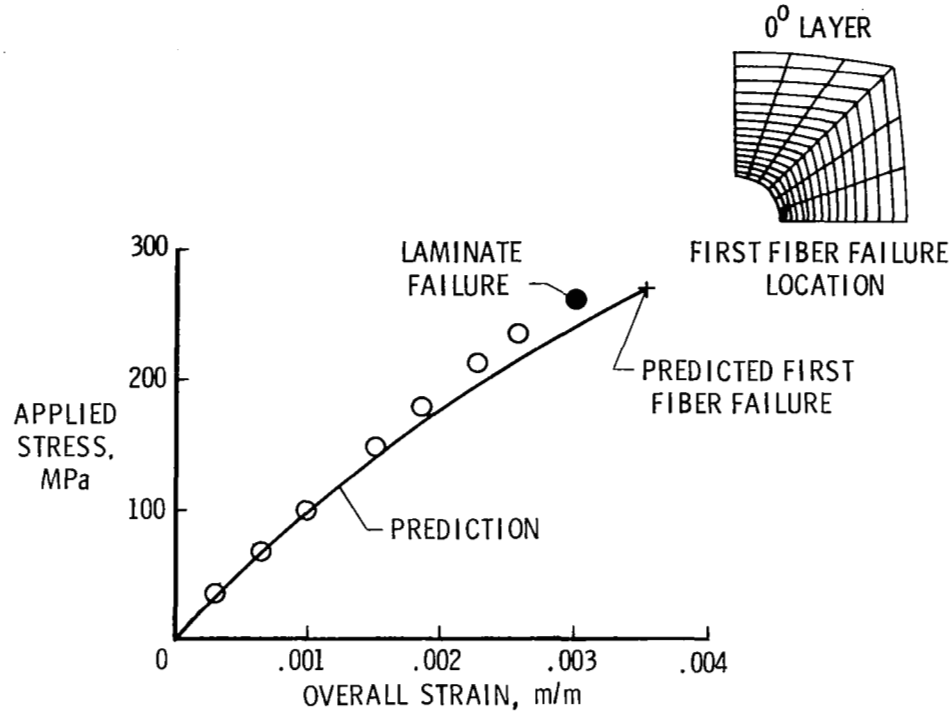

Figure 18.- Stress-strain response to failure of $[0/\pm45]_s$ laminate with circular hole. 2a = 25.4 mm; w = 102 mm.

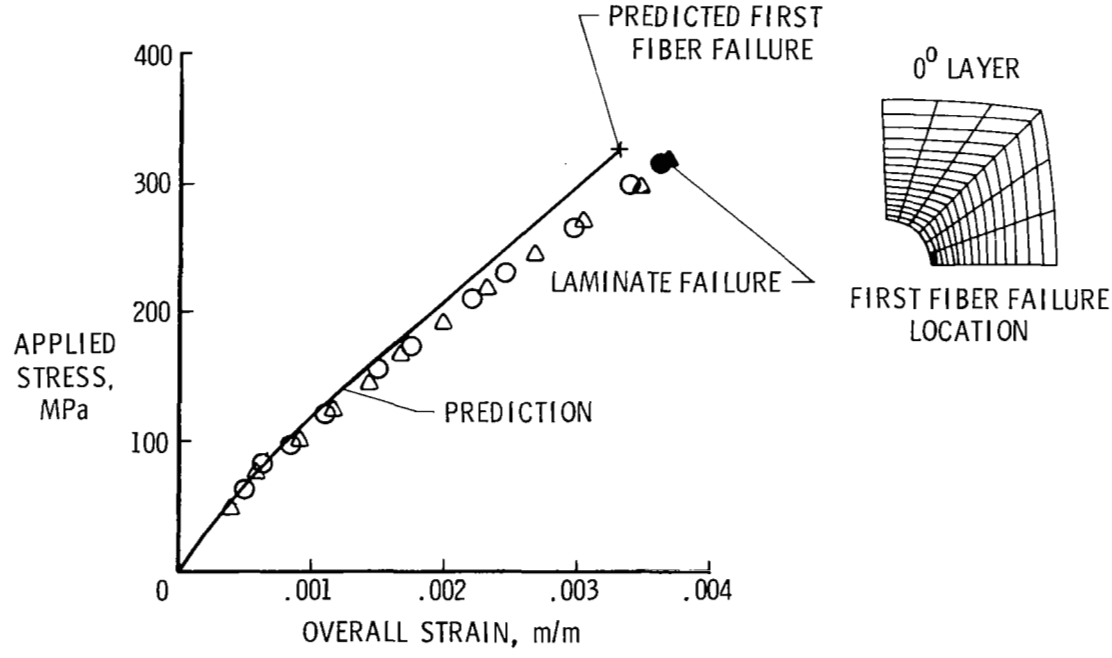

Figure 19.- Stress-strain response to failure of $[0_2/\pm45]_s$ laminate with circular hole. 2a = 25.4 mm; w = 102 mm.

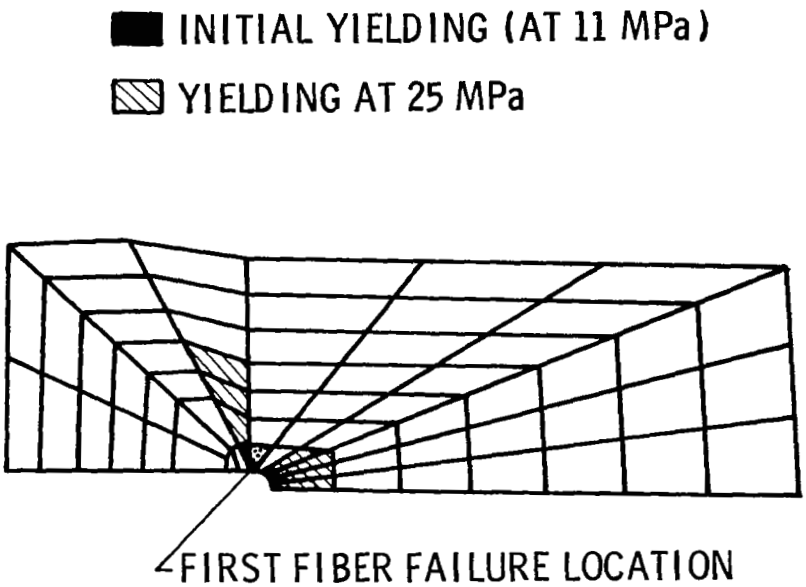

(a) Yield pattern at notch tip.

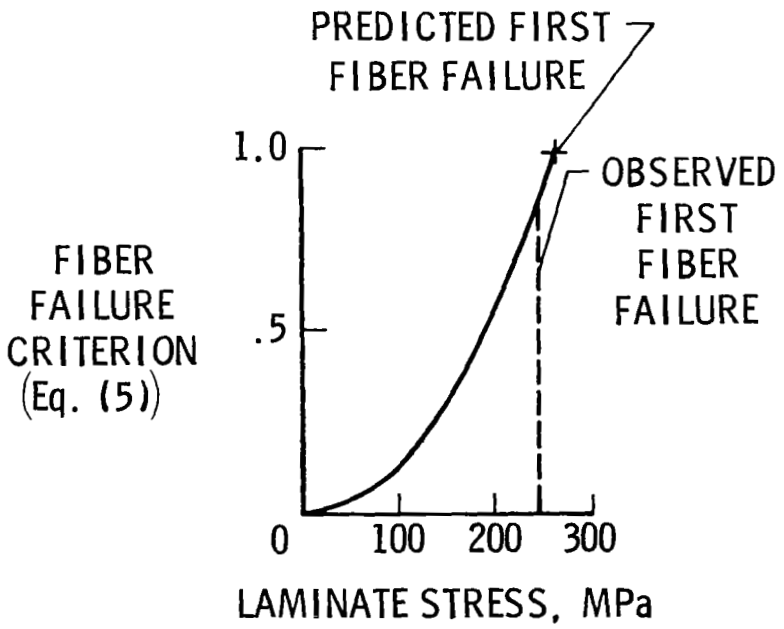

(b) First fiber failure.

Figure 20.- First fiber failure of monolayer specimen. 2a = 19 mm; w = 78 mm.

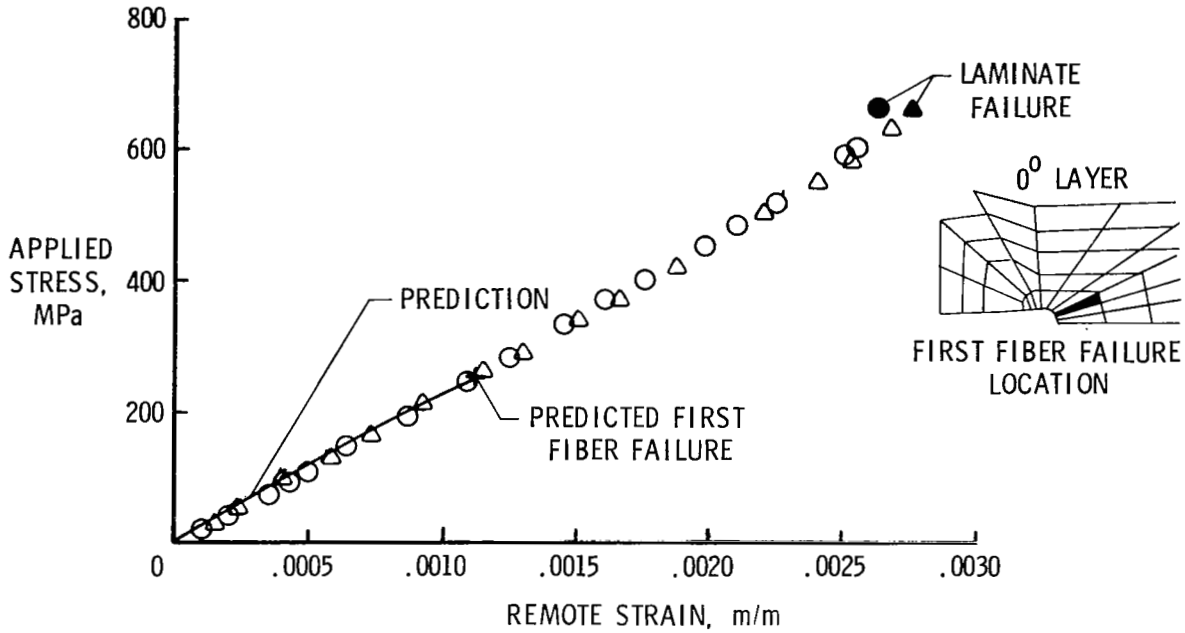

Figure 21.- Stress-strain response to failure of $[0]_6$ laminate with crack-like slit. 2a = 15 mm; w = 51 mm.

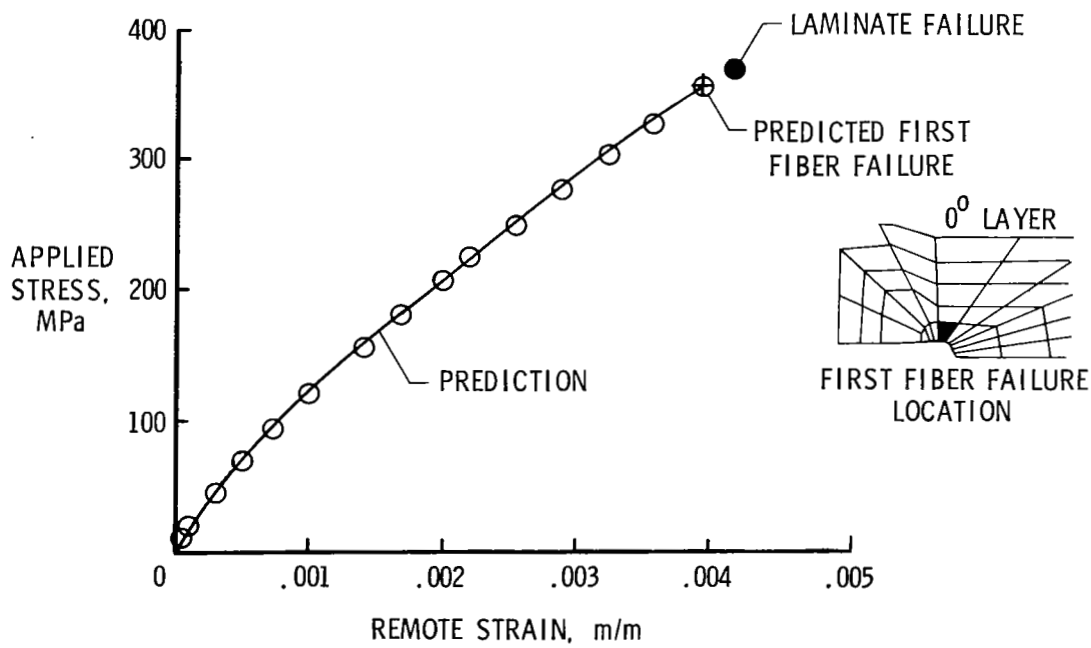

Figure 22.- Stress-strain response to failure of $[0/\pm45]_s$ laminate with crack-like slit. 2a = 10 mm; w = 102 mm.

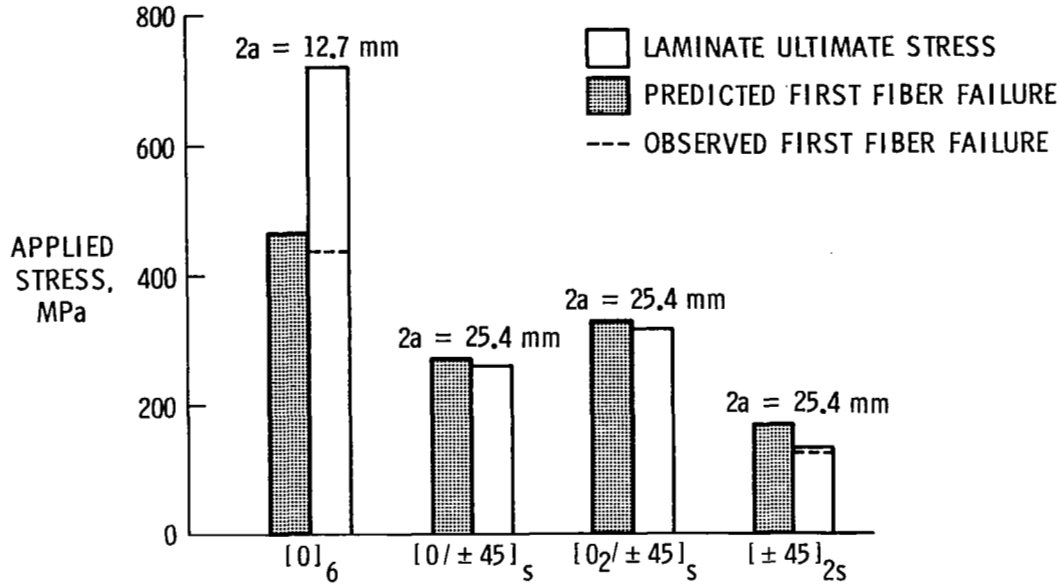

Figure 23.- First fiber failure compared with laminate ultimate stress for specimens with circular holes. w = 102 mm.

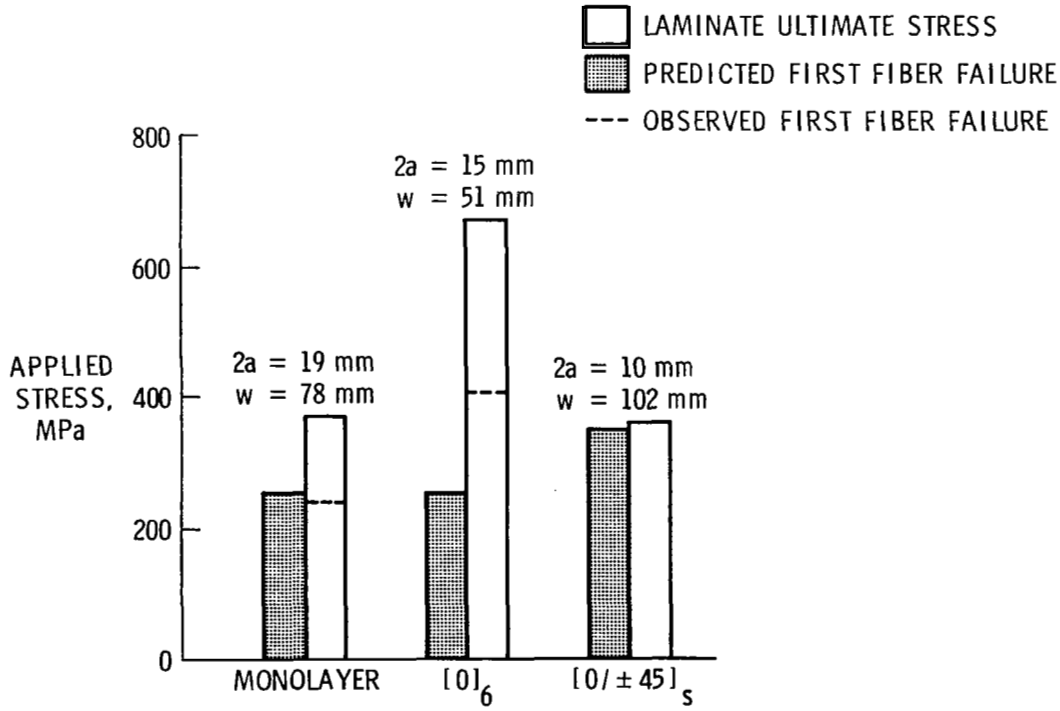

Figure 24.- First fiber failure compared with laminate ultimate stress for specimens with crack-like slits.

1. Report No.	2. Government Accession No.	3. Recipient's Catalog No.
NASA TP-2187		

4. Title and Subtitle	5. Report Date
EXPERIMENTAL AND ANALYTICAL INVESTIGATION OF THE FRACTURE PROCESSES OF BORON/ALUMINUM LAMINATES CONTAINING NOTCHES	September 1983
	6. Performing Organization Code: 505-33-33-05
7. Author(s): W. S. Johnson, C. A. Bigelow, and Y. A. Bahei-El-Din	8. Performing Organization Report No.: L-15574
	10. Work Unit No.
9. Performing Organization Name and Address: NASA Langley Research Center, Hampton, VA 23665	11. Contract or Grant No.
	13. Type of Report and Period Covered: Technical Paper
12. Sponsoring Agency Name and Address: National Aeronautics and Space Administration, Washington, DC 20546	14. Sponsoring Agency Code

15. Supplementary Notes

W. S. Johnson and C. A. Bigelow: Langley Research Center, Hampton, Virginia.
Y. A. Bahei-El-Din: University of Cairo, Cairo, Egypt.

16. Abstract

The purpose of this report is to enhance understanding of the fracture process of metal matrix composites, boron/aluminum composites specifically. These composites experience widespread yielding of the matrix material during the fracture process. This plasticity complicates the analysis of the composites containing notches. This report presents experimental results for five laminate orientations of boron/aluminum composites containing either circular holes or crack-like slits. Specimen stress-strain behavior, stress at first fiber failure, and ultimate strength were determined. Radiographs were used to monitor the fracture process. The specimens were analyzed with a three-dimensional elastic-plastic finite-element model. The first fiber failures in notched specimens with $[\pm 45]_{2s}$, $[0/\pm 45]_{s}$, and $[0_2/\pm 45]_{s}$ laminate orientations occurred at or very near the specimen ultimate strength. For notched unidirectional specimens, the first fiber failure occurred at approximately one-half of the specimen ultimate strength. Acoustic emission events correlated with fiber breaks in unidirectional composites, but did not for other laminates. Circular holes and crack-like slits of the same characteristic length were found to produce approximately the same strength reduction. The predicted stress-strain responses and stress at first fiber failure compared very well with test data for laminates containing 0° fibers and reasonably well for $[\pm 45]_{2s}$ laminates.

17. Key Words (Suggested by Author(s))	18. Distribution Statement
Metal matrix composites Fracture Boron/aluminum Radiography Elastic-plastic finite-element analysis Fiber failure Constituent material model	Unclassified - Unlimited Subject Category 24

19. Security Classif. (of this report)	20. Security Classif. (of this page)	21. No. of Pages	22. Price
Unclassified	Unclassified	43	A03

For sale by the National Technical Information Service, Springfield, Virginia 22161

NASA-Langley, 1983

3 1 1U,C, 830830 S00903DS
DEPT OF THE AIR FORCE
AF WEAPONS LABORATORY
ATTN: TECHNICAL LIBRARY (SUL)
KIRTLAND AFB NM 87117